U.S. DEPARTMENT OF ENERGY

PNNL-21214

Prepared for the U.S. Department of Energy
under Contract DE-AC05-76RL01830

Numerical Modeling of ^{90}Sr and ^{137}Cs Transport from a Spill in the B-Cell of the 324 Building, Hanford Site 300 Area

ML Rockhold
DH Bacon
VL Freedman
MJ Lindberg
RE Clayton

March 2012

Pacific Northwest NATIONAL LABORATORY

Proudly Operated by Battelle Since 1965

DISCLAIMER

PACIFIC NORTHWEST NATIONAL LABORATORY
operated by
BATTELLE
for the
UNITED STATES DEPARTMENT OF ENERGY
under Contract DE-AC05-76RL01830

Printed in the United States of America

Available to DOE and DOE contractors from the
Office of Scientific and Technical Information,
P.O. Box 62, Oak Ridge, TN 37831-0062;
ph: (865) 576-8401
fax: (865) 576-5728
email: reports@adonis.osti.gov

Available to the public from the National Technical Information Service,
U.S. Department of Commerce, 5285 Port Royal Rd., Springfield, VA 22161
ph: (800) 553-6847
fax: (703) 605-6900
email: orders@ntis.fedworld.gov
online ordering: http://www.ntis.gov/ordering.htm

This document was printed on recycled paper.
(9/2003)

PNNL-21214

Numerical Modeling of ^{90}Sr and ^{137}Cs Transport from a Spill in the B-Cell of the 324 Building, Hanford Site 300 Area

ML Rockhold
DH Bacon
VL Freedman
MJ Lindberg
RE Clayton

March 2012

Prepared for
the U.S. Department of Energy
under Contract DE-AC05-76RL01830

Pacific Northwest National Laboratory
Richland, Washington 99352

Summary

In October 1986, a spill of a highly radioactive waste stream containing cesium (^{137}Cs) and strontium (^{90}Sr) occurred in the B-Cell of the 324 Building in the 300 Area of the Hanford Site. The spill is estimated to have contained approximately 1.3 million curies of radioactivity. An unknown fraction of this spill was lost to the subsurface through a leak in the sump in the floor of B-Cell.

To characterize the extent of contamination under the 324 Building, a pit was excavated on the north side of the building in 2010 by Washington Closure Hanford LLC (WCH). Horizontal closed-end steel access pipes were installed under the foundation of the building from this pit and were used for measuring temperatures and exposure rates under the B-Cell. The deployed sensors measured elevated temperatures of up to 61 °C (142 °F) and exposure rates of up to 8,900 R/hr. WCH suspended deactivation of the facility because it recognized that building safety systems and additional characterization data might be needed for remediation of the contaminated material. The characterization work included additional field sampling, laboratory measurements, and numerical flow and transport modeling.

Laboratory measurements of sediment physical, hydraulic, and geochemical properties were performed by Pacific Northwest National Laboratory (PNNL) and others. Geochemical modeling and subsurface flow and transport modeling also were performed by PNNL to evaluate the possible extent of contamination in the unsaturated sand and gravel sediments underlying the building. Historical records suggest that the concentrated ^{137}Cs- and ^{90}Sr-bearing liquid wastes that were spilled in B-Cell were likely from a glass-waste repository testing program associated with the Federal Republic of Germany (FRG). Incomplete estimates of the aqueous chemical composition (no anion data provided) of the FRG waste solutions were entered into a geochemical speciation model and were charge balanced with nitrate to estimate waste composition. Additional geochemical modeling was performed to evaluate reactions of the waste stream with the concrete foundation of the building prior to the stream entering the subsurface.

One-dimensional (1-D) and three-dimensional (3-D) flow and transport simulations were performed using the STOMP simulator. Vertically oriented 1-D reactive transport simulations were conducted for three different water release scenarios using a reaction network that considered aqueous speciation, ion exchange, and mineral precipitation and dissolution reactions. The 1-D simulations were performed to evaluate the potential influence of waste chemistry and ion-exchange processes on vertical radionuclide transport for a range of possible water release rates. Three-dimensional simulations were also performed using a linear adsorption isotherm (K_d) model to provide estimates of the possible extent of contamination in both the vertical and lateral directions underlying the B-Cell. K_d values in the 3-D model were adjusted, although not optimized, to obtain improved correspondence between model results and field observations for two water release scenarios.

The 1-D and 3-D models yield differing results in terms of the predicted depths to peak concentrations and the maximum depths of penetration of the contaminants. This is an expected result because of differences in dimensionality and processes represented by the models and because of uncertainties in water release rates and composition of the leaked fluids. Both models predict transport of contaminants into the vadose zone but not reaching the saturated zone. The 1-D reactive transport model results, which are assumed to be conservative, suggest that the highest concentrations of ^{137}Cs may be located immediately below the foundation of the B-Cell and that ^{137}Cs contamination may extend 3–7 m below the foundation, depending on the assumed water release scenario. The 1-D reactive

transport results suggest that peak concentrations of ^{90}Sr may be located 1–3 m below the foundation and that ^{90}Sr contamination may extend 4–11 m below the foundation, again depending on the assumed water release rate. The depth to the average position of the water table is approximately 15 m. In contrast, the 3-D K_d-based model results suggest that for both ^{137}Cs and ^{90}Sr, peak concentrations may be located 1–2 m below the foundation, and nearly all of the contamination may be contained within the upper 3 m of the sediment profile. The simulated peak ^{90}Sr concentrations for the 3-D K_d-based model are lower in magnitude and approximately 0.5 m deeper in the profile below the foundation of the B-Cell, relative to the simulated peak ^{137}Cs concentrations.

The actual volume of water associated with the leak, the volumes of water used in subsequent washing operations, the chemical composition of the waste stream, and the properties of the sediments underlying the 324 Building are all highly uncertain. Consequently, the model-based estimates of contaminant distributions are also highly uncertain. With additional field and laboratory characterization data, it might be possible to reduce and better quantify some of these uncertainties, evaluate risk associated with remediation activities, and provide more reliable quantitative estimates of contaminant distribution for waste disposal planning.

Field data and simulation results suggest that the pit excavated on the north side of the 324 Building to provide access for direct-push sampling efforts is resulting in increased moisture under the building, due to exposure to natural precipitation that is infiltrating into the subsurface. If excavation of the contaminated sediments under the B-Cell proceeds relatively quickly, say within 1-2 years, then this increasing moisture may be of little or no consequence. However, if the excavation and removal of contaminated sediments under the B-Cell takes longer, then the increased moisture could eventually result in mobilization and transport of contaminants to groundwater. There are currently no groundwater monitoring wells near and downgradient of the 324 Building.

In general, site decommissioning and demolition activities in the 300 Area and elsewhere at Hanford have the potential for increasing natural groundwater recharge rates due to surface disturbance. Recharge is the primary driving force for transporting contaminants in the vadose zone to the underlying aquifer.

Acknowledgments

Thanks to Matt Perrott of Washington Closure Hanford LLC for providing data and references used in this report. Walt Josephson of Worley Parsons is acknowledged for providing Monte-Carlo N-Particle calculation results. Thanks also to Andrea Currie and Kathy Neiderhiser for editorial and text processing support. Finally, thanks to Mike Fayer and Xingyuan Chen for reviewing the document.

Acronyms and Abbreviations

1-D	one-dimensional
3-D	three-dimensional
CAD	computer-assisted design
CEC	cation-exchange capacity
Ci	curie(s)
cm	centimeter(s)
DOE	U.S. Department of Energy
EPA	U.S. Environmental Protection Agency
FRG	Federal Republic of Germany
ft	foot, feet
g	gram(s)
gal	gallon(s)
GM	Geiger-Müller detector for ionizing radiation
HEIS	Hanford Environmental Information System
IFRC	Integrated Field Research Challenge
K_d	sorption coefficient
K_s	hydraulic conductivity
L	liter(s)
LANL	Los Alamos National Laboratory
µCi	microcurie(s)
m	meter(s)
mm	millimeter(s)
MCL	maximum contaminant level
MCNP	Monte-Carlo N-Particle: a particle transport code developed by LANL
meq	milliequivalent
msG	muddy sandy gravel
NaOAc	sodium acetate
NH_4OAc	ammonium acetate
pCi	picocurie(s)
PNNL	Pacific Northwest National Laboratory
R/hr	rad(s) per hour
STOMP	Subsurface Transport Over Multiple Phases: a flow and transport simulator developed by PNNL
WCH	Washington Closure Hanford LLC
WIDS	Waste Information Data System
wk	week(s)

Contents

Figures

Tables

1.0 Introduction

The 324 Building in the 300 Area of the Hanford Site in southeastern Washington State was used for chemical and radionuclide processing associated with nuclear weapons production during the Cold War Era. After the cessation of these activities, the facility was used for a variety of purposes including experiments in which highly radioactive wastes were stabilized into glass waste forms for testing in nuclear waste repository programs. A hot cell within the 324 Building, called the B-Cell, was used for handling radionuclides that were associated with some of these programs.

The B-Cell within the 324 Building is located approximately 300 m from the Columbia River shoreline (Figure 1.1). Both the 324 Building and the 3718P Building to the east were built on top of the former 618-6 burial ground. The contents of the 618-6 burial ground were excavated and moved to the outlying 618-10 burial ground in 1962 to make room for construction of the 324 Building, according to the Waste Information Data System (WIDS). Figure 1.2 is an historical photograph of the site where the 324 Building was constructed. From this photograph, the sediments under the 324 Building consist of a thin layer of relatively uniform eolian sand underlain by a thicker deposit of coarser and much more heterogeneous flood-deposited and gravel-dominated sediments of the Hanford formation. The reader is referred to Bjornstad et al. (2009) for more information regarding Hanford formation sediments in the 300 Area.

Historical records indicate that in October 1986, approximately 510 L of a concentrated liquid cesium-137 (^{137}Cs) and strontium-90 (^{90}Sr) waste stream was spilled onto the floor of the B-Cell.[1] It is estimated that this spill contained ~1.3 million curies of radioactivity. Some fraction of the spill may have been recovered, but an unknown quantity was lost into the subsurface beneath the 324 Building through a leak in the sump in the floor of the B-Cell. Unknown quantities of water were used immediately after the spill, and at various other times following the spill, to wash items contained in the B-Cell (MW Perrott, WCH, private communication, January 2011). Wastes being removed from B-Cell were also grouted and in the course of the grouting activities, sufficient grout was spilled on the floor of the B-Cell to completely fill the sump with solidified grout. Although unintentional, this spilling of grout is thought to have effectively stopped any further release of waste through the B-Cell sump, at some undetermined time prior to 1992. For the purposes of numerical modeling it is assumed that no further contamination was released from the B-Cell after 1992.

The base of the concrete foundation underlying the B-Cell is approximately 15 m above the average elevation of the water table in the 300 Area. The closest groundwater monitoring well to the B-Cell was well 399-3-11, which was within the footprint of the 3718P Building that was located just east of the 324 Building, as shown in Figure 1.1. ^{90}Sr concentration data that were monitored in well 399-3-11 are shown in Figure 1.3.[2] The maximum contaminant level (MCL) for ^{90}Sr, promulgated under the federal National Primary Drinking Water Regulations for radionuclides (40 CFR 141.66), is 8 pCi/L. Concentrations or activities of ^{90}Sr exceeding the MCL were detected prior to the 1986 spill in B-Cell, as well as one time after the spill. The most recent measurements indicated ^{90}Sr concentrations were less than one-half the MCL and declining. Well 399-3-11 was decommissioned in 2010, and ^{90}Sr has not been

[1] WCH, 2011, *Characterization of the Soil Contamination Under 324 B Cell*, Calculation No. 0300X-CA-N0140, Rev. 1., Washington Closure Hanford, Richland, Washington.
[2] Source: data from the Hanford Environmental Information System.

detected in any other 300 Area groundwater monitoring wells (Hartman et al. 2007). It is assumed that the ^{90}Sr previously detected in groundwater at well 399-3-11 was associated with other former waste disposal sites or accidental spills (e.g., UPR-300-1; WIDS) and was not from the B-Cell leak (Hartman et al. 2007).

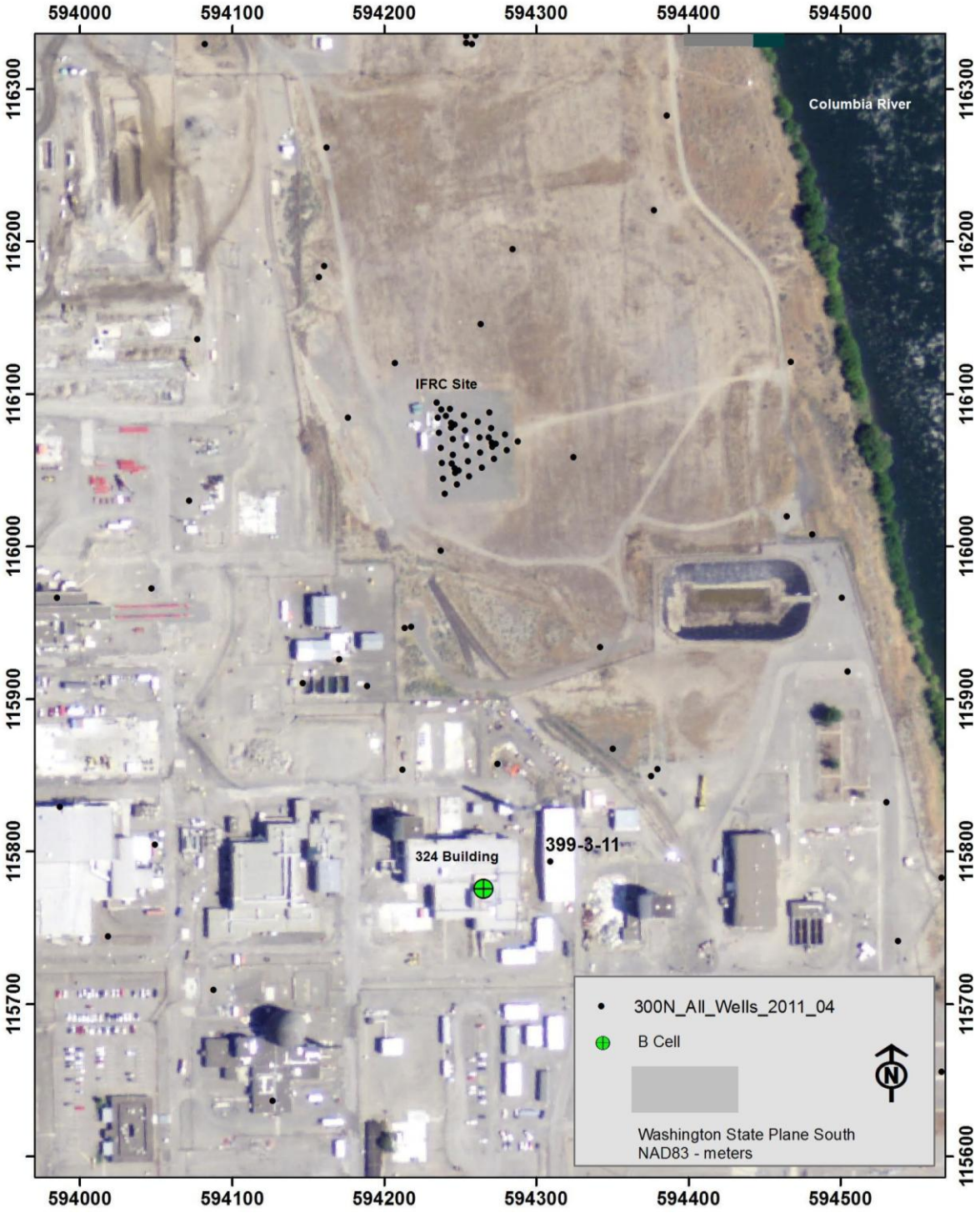

Figure 1.1. Aerial photograph of the 324 Building and other 300 Area buildings that existed prior to demolition, and locations of groundwater monitoring wells.

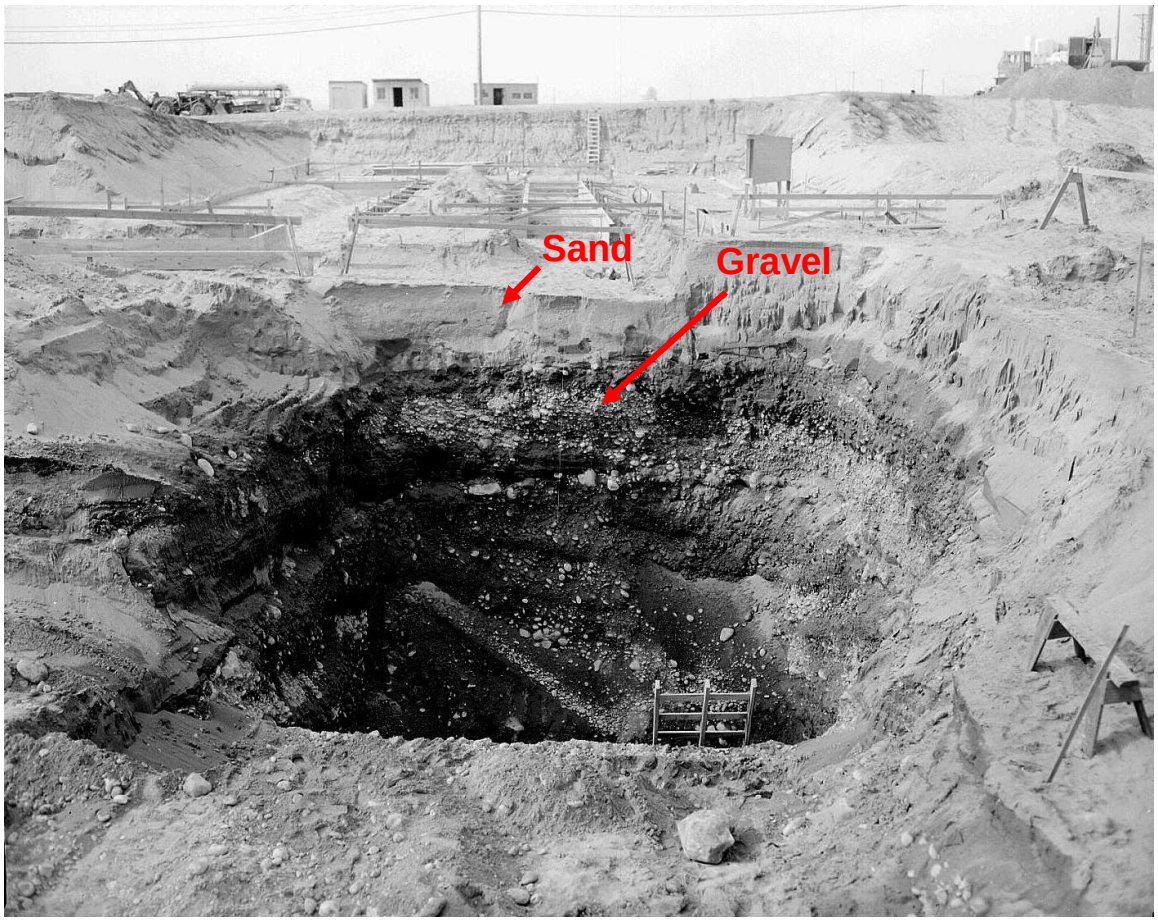

Figure 1.2. Historical photograph of the site where the 324 Building was constructed, showing a thin layer of relatively uniform eolian sand underlain by a thicker layer of coarser and much more heterogeneous gravel-dominated, flood-deposited sediments of the Hanford formation.

Most of the former chemical and radionuclide processing facilities in the 300 Area have now been demolished as part of Hanford Site cleanup and decommissioning activities by Washington Closure Hanford LLC (WCH). Prior to decommissioning of the 324 Building, WCH excavated a pit on the north side of the building and subcontracted others to use a Geoprobe system to install eight closed-end horizontal access pipes in a fan-shaped pattern under the B-Cell. Pacific Northwest National Laboratory (PNNL) deployed sensors within these access pipes and detected elevated temperatures of up to 61 °C (142 °F) and exposure rates of up to 8,900 R/hr. These extremely high rates are considered to be lethal to human receptors within a few minutes of direct exposure.

After the initial subsurface characterization effort, WCH contracted with others to calculate radionuclide activities from the exposure rate measurements. Two additional deeper closed-end access pipes were also installed, and geophysical logging was performed in these two deep access pipes and four of the original horizontal access pipes to measure volumetric water content and gamma energy emissions. Two additional shallow open-end access pipes were also installed to collect physical samples at two locations/depths immediately below the B-Cell sump. These two physical samples were analyzed by PNNL for bulk chemistry and radionuclide activity. Laboratory analyses were also performed to measure physical, hydraulic, and sorption properties for two sediment samples collected from a pit excavated on

the north side of the 324 Building. Further details regarding site characterization data are provided in Section 2 of this report.

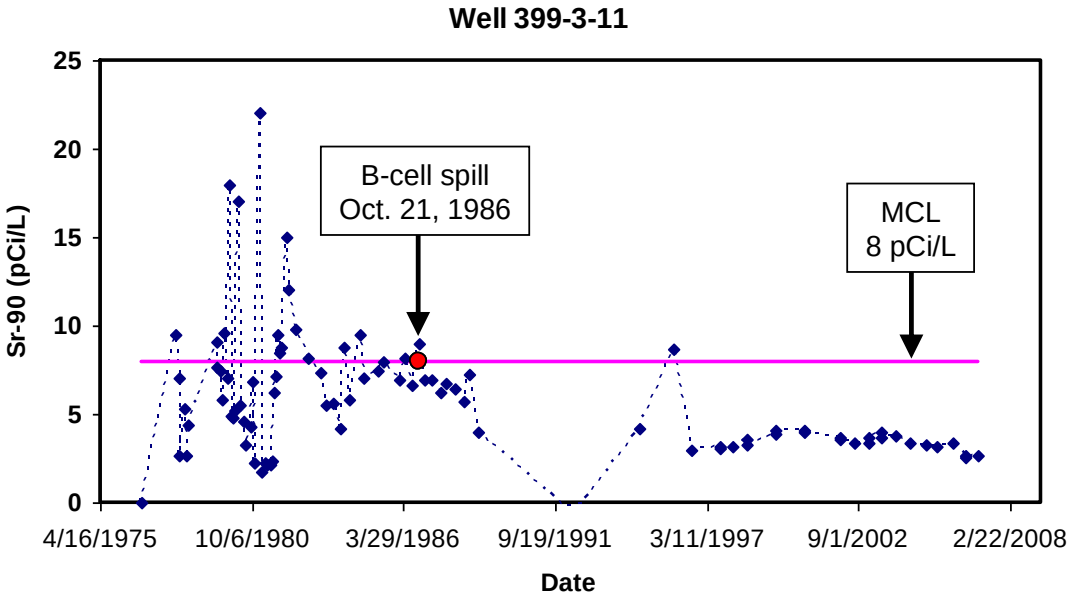

Figure 1.3. Strontium-90 activities monitored in groundwater samples from well 399-3-11, located approximately 50 m east of the B-Cell. Well 399-3-11 was decommissioned in 2010. Data are from HEIS with one apparent outlier of 4700 pCi/L from May 16, 1978 removed from the plot. The maximum contaminant level (MCL) for ^{90}Sr is 8 pCi/L.

In general, characterization data for the sediments in the vicinity of and underlying the 324 Building are very limited. However, the DOE Office of Science is supporting an Integrated Field Research Challenge (IFRC) Site in the 300 Area, located approximately 300 m to the north of the B-Cell, shown in Figure 1.1. This field experimental research site is operated for DOE by PNNL to investigate flow, transport, and mass transfer behavior of uranium associated with former 300 Area waste disposal ponds.

Sediment and aquifer characterization data and experimental results from the IFRC site provide a valuable resource for other contaminant transport investigations in the 300 Area and elsewhere along the Columbia River corridor. Some of the sediment characterization data generated by the IFRC project were referenced and utilized in this report.

PNNL was contracted by WCH to provide numerical modeling support to help inform decisions regarding future site decommissioning and excavation activities at the 324 Building. PNNL's work scope for this effort was to 1) develop an initial conceptual model for the release of ^{137}Cs and ^{90}Sr from the B-Cell into the shallow subsurface (vadose zone) underlying the 324 Building, 2) perform numerical modeling of water flow and the transport and fate of ^{137}Cs and ^{90}Sr using the STOMP simulator (White and Oostrom 2006; White and McGrail 2005), and 3) estimate the possible extent of migration of these radionuclides.

This report documents work performed by both PNNL and others in support of WCH decommissioning activities for the 324 Building. The report is organized as follows. Section 1 (this

section) provides an introduction and overview of the contamination problem associated with the B-Cell leak. Section 2 describes most of the available characterization data. Section 3 presents numerical flow and transport modeling results and comparisons with field data. Section 4 closes with conclusions and recommendations. Supplemental information is provided in the appendix.

2.0 Characterization Data

Various types of field data have been collected from the subsurface underlying the B-Cell by several subcontractors to WCH, including PNNL, to characterize contaminant distributions. Supporting laboratory analyses have also been performed to characterize sediment properties. This section summarizes some of the data that have been collected to date.

2.1 Exposure Rate and Temperature Data

Prior to decommissioning and demolition of the 324 Building, WCH excavated a pit on the north side of the building and subcontracted others to use a Geoprobe system to successfully install eight horizontal closed-end steel access pipes in a fan-shaped pattern under the B-Cell (Figure 2.1). Exposure rate and temperature measurements were made in these access pipes to provide initial estimates of the nature and extent of contamination under the B-Cell.

Figure 2.1. A portion of the pit excavated on the north side of the 324 Building and near-horizontal steel access pipes installed using a Geoprobe system. These access pipes have been used for exposure rate and temperature measurements and for neutron moisture and spectral gamma logging.

Figure 2.2 shows AutoCAD renditions of the B-Cell and the original eight access pipes that were installed from the pit shown in Figure 2.1. The symbols along each pipe shown in Figure 2.2 represent the log-scaled exposure rate measurements.

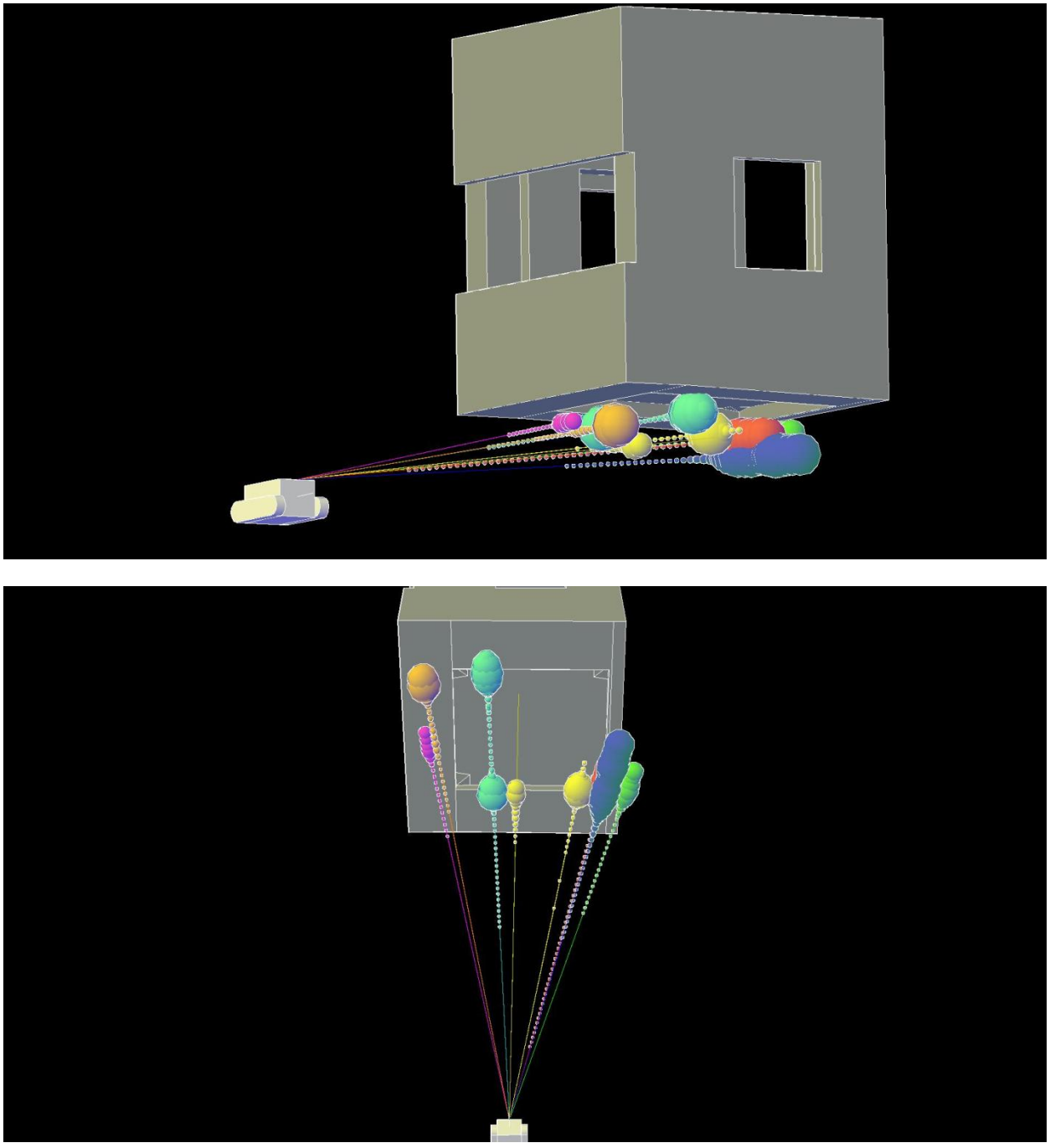

Figure 2.2. AutoCAD renditions of the B-Cell and the original eight access pipes installed under the B-Cell. The symbols indicate log-scaled exposure rate measurements.

Figure 2.3 shows exposure rates that were measured in these eight access pipes.[1] Exposure rates of up to 8,900 R/hr were detected. As noted previously, these high rates are considered to be lethal to human receptors within a few minutes of direct exposure. Radionuclide activities were also estimated from the exposure rate data using modeling calculations based on the ORIGEN (ORNL 1980) and Monte-Carlo N-Particle (MCNP) codes (LANL 2005). These calculated activities are discussed in more detail in Section 3.

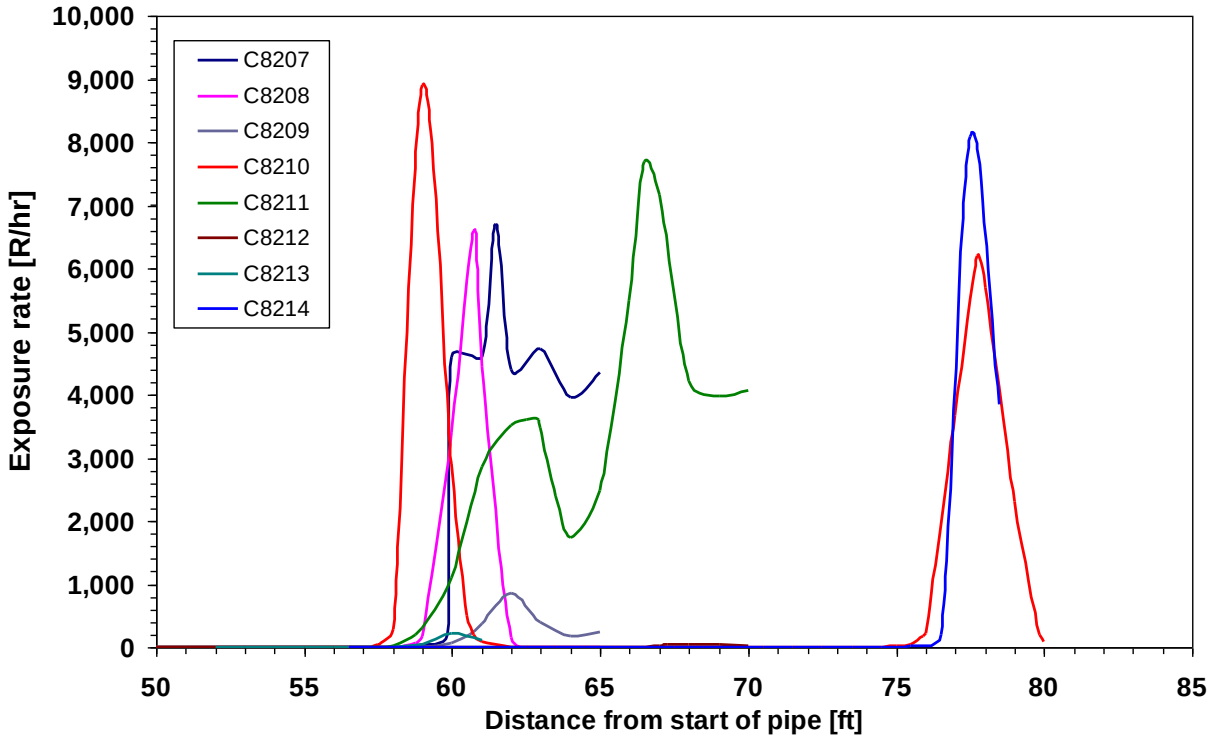

Figure 2.3. Measured exposure rates in eight near-horizontal access pipes installed under B-Cell.

The peaks in the measured exposure rates approximately underlie the locations of the expansion joints in the B-Cell floor. Based on this spatial distribution of exposure rates and detailed inspection of construction drawings, the current interpretation is that the leak from the B-Cell sump spread laterally along a felt liner on the floating concrete foundation of the B-Cell. After the leak reached the expansion joint, it migrated vertically downward into the underlying sediments. Unknown quantities of water were used immediately after the leak and at later times to wash the floor of the B-Cell. This added water would have transported ^{137}Cs and ^{90}Sr deeper into the underlying sediments. As noted previously, the B-Cell sump was inadvertently grouted sometime prior to1992, after which it was assumed that no further contamination was transported from B-Cell into the subsurface.

Figure 2.4 shows the measured exposure rate data for one of the access pipes, together with temperature and neutron count data. Note that two exposure rate meters (RO-7 and AMMG) with

[1] PNNL, 2011, Results of screening measurements of geoprobe pipes, Pacific Northwest National Laboratory, Richland, Washington; unpublished data.

different sensitivities were employed, and they yielded similar results. Elevated temperatures of up to 61 °C (142 °F) were detected. These elevated temperatures are clearly a result of heat generated by radioactive decay.

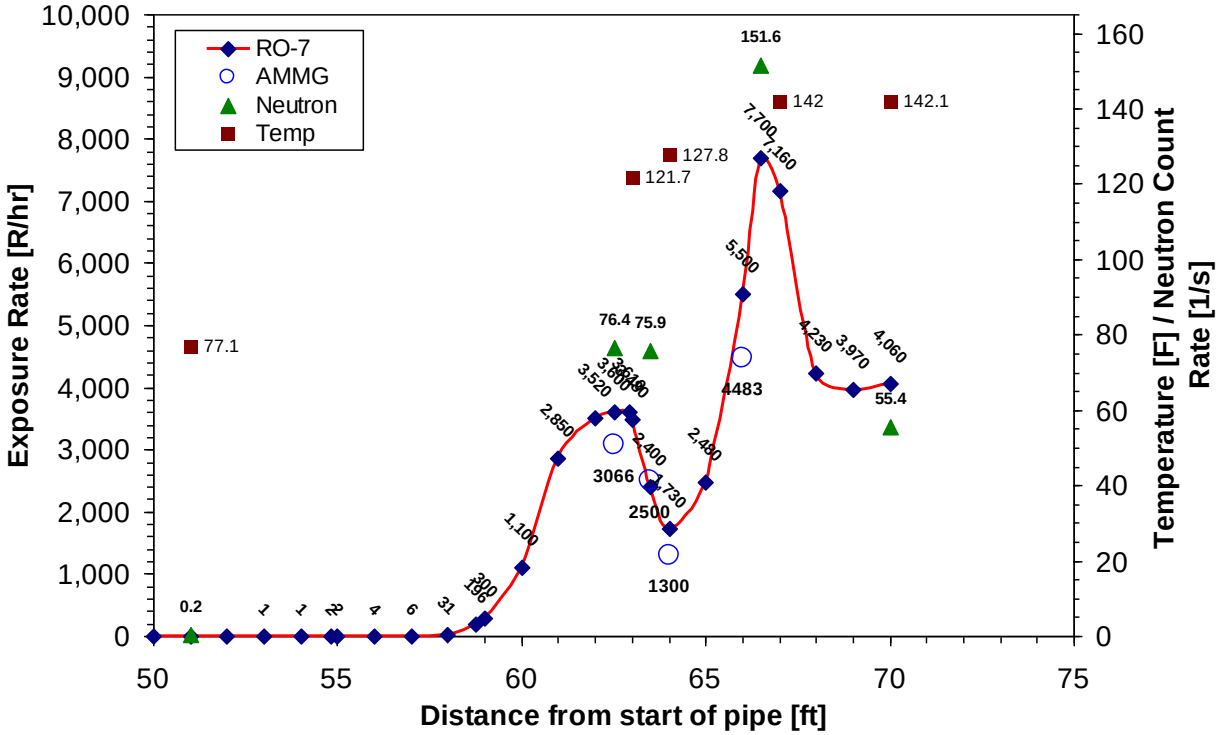

Figure 2.4. Measured exposure rate, temperature, and neutron count data from one of the original eight horizontal access pipes installed under B-Cell.

2.2 Neutron Moisture Data and Computed Radionuclide Activities

EnergySolutions Federal Services, Inc. performed neutron-moisture logging in four of the original eight horizontal access pipes installed under B-Cell.[1] EnergySolutions also logged neutron moisture measurements in two closed-end access pipes that were installed later and at steeper angles from a site located approximately 10 m to the east of the origin of the horizontal access pipes. Figure 2.5 depicts the locations of these six access pipes and the measurement locations for volumetric water content data obtained from neutron-moisture logging.

Figure 2.6 shows annotated plots of the volumetric water content data versus distance from the start of the pipe and with elevation for four of the horizontal access pipes. The volumetric water content profiles exhibit several interesting features. The pit used for access in sampling activities was excavated in October 2010, after removal of a maintenance shed and pad that had previously covered that area (MW Perrott, WCH, private communication, August 2011). As shown in Figure 2.1, the near-horizontal access pipes are exposed to air within the pit before they enter the sediment. Hence the water content

[1] EnergySolutions, 2011, Direct Push Activities and Logging Results for Probeholes near the 324 Building at the Hanford Site, Document No. C013324A00CN034-05-002-001A, EnergySolutions Federal Services, Inc., Richland, Washington; unpublished data.

values shown for short pipe distances are very low, indicating where the pipe is surrounded by air rather than moist sediment. Water content values become elevated at pipe distances that correspond to locations just past the edge of the pit where the neutron probe first enters the sediment.

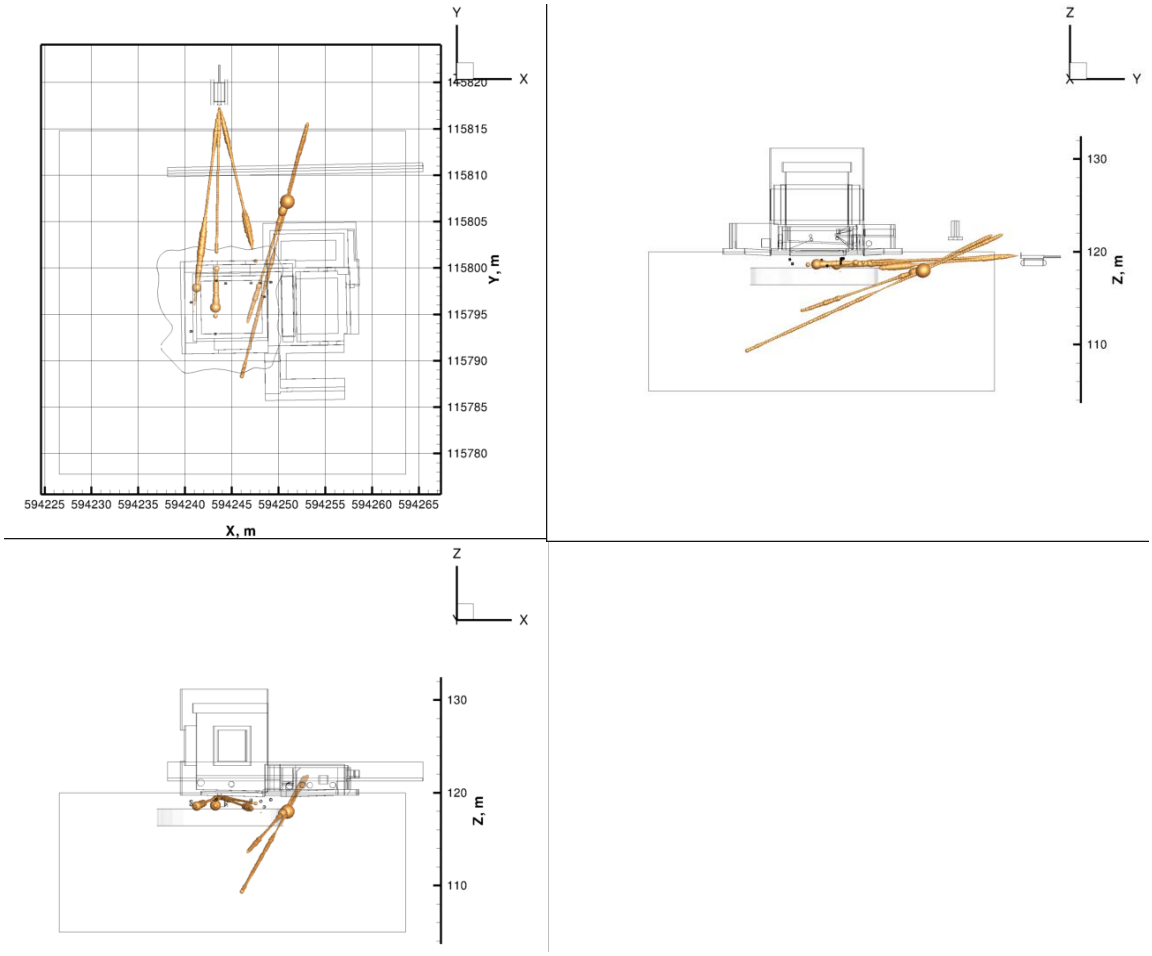

Figure 2.5. Spatial locations of six Geoprobe access tubes used for neutron-moisture measurements and locations of these measurements. Symbol size is scaled by moisture content.

The elevated water content values between pipe distances of approximately 6 and 12 ft are interpreted to be a result of the exposed trench allowing water to enter the sediments under the newly exposed edge of the building. This interpretation was corroborated by numerical experiments. The elevated water content values near the edge of the pit are of some concern and suggest that the pit is allowing additional water from natural precipitation to enter the sediment profile near the area of contamination. It should also be noted that a water main was apparently flushed in November 2010, which allowed an estimated several hundred gallons of water to enter the pit (MW Perrott, WCH, private communication, September 2011). This water release could also have contributed to higher water content values near the edge of the pit.

As shown in Figure 2.6, after this region of elevated water content between pipe distances of 6 to 12 ft, the values then decrease with increasing pipe distance. Near-constant volumetric water content values of about 4% were measured between pipe distances of 20 to 40 ft. After 40 ft, water content

increases again, followed by a very dry region at a pipe distance of about 52 ft for three of the four access pipes. The dry region is interpreted to be a result of decay heat.

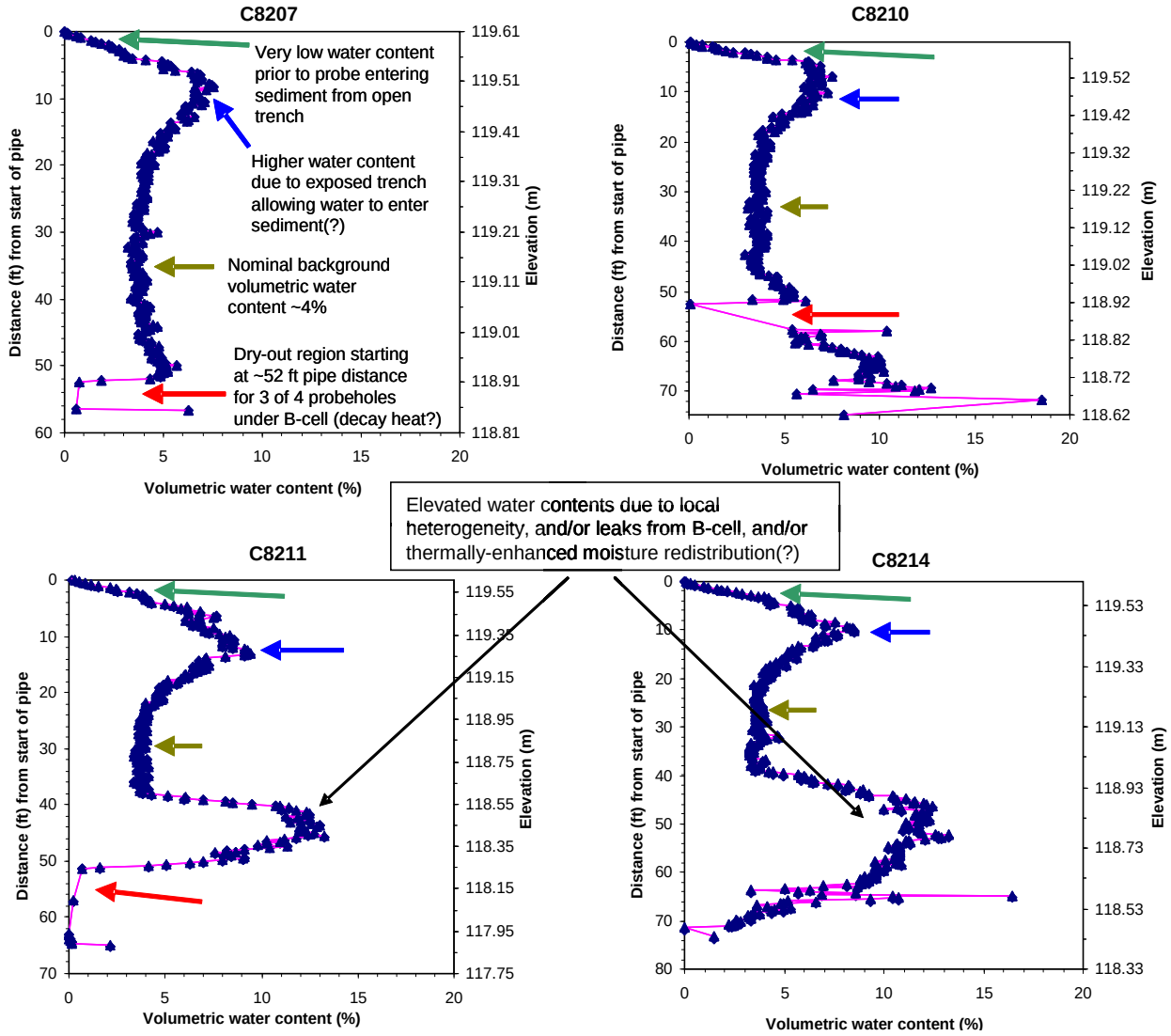

Figure 2.6. Volumetric water content data measured in four near-horizontal access pipes installed under B-Cell and annotated interpretation.

This dry region, as well as the region of elevated water contents between pipe distances of 40 and 52 ft, may be a result of, or influenced by, thermally enhanced moisture redistribution. It is also possible, however, that the regions of elevated water content could simply be finer-grained sediments such as rip-up clasts of the Ringold Formation (Bjornstad et al. 2009).

Figure 2.7 shows volumetric water content data as a function of elevation for all six of the access pipes logged by the neutron tool for the upper 3 m of the sediment profile. Because the access pipes are not vertically oriented, and because the data are influenced by sediment heterogeneity as well as by water additions from the leak and/or recharge from natural precipitation, these profiles must be interpreted

carefully. Determining the influence of water additions from leaks versus natural recharge in this setting is complicated by the spatially variable and changing nature of the surface cover because buildings and parking lots around the 324 Building have been removed over the past several years during site decommissioning.

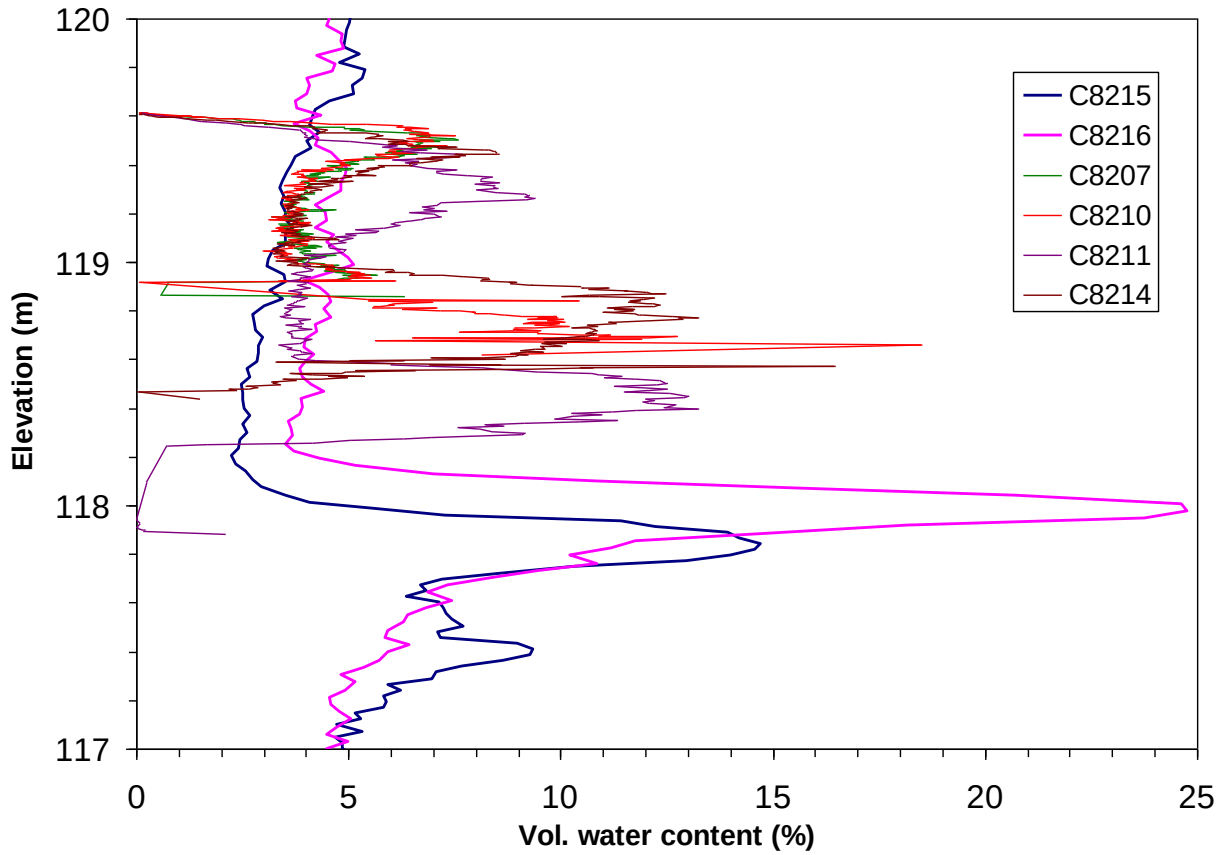

Figure 2.7. Volumetric water content data as a function of elevation, measured using a neutron logging tool for six access pipes.

A period of approximately 25 years passed between 1986 when the B-Cell leak occurred and 2010 when neutron logging was performed to measure volumetric water content under the B-Cell. This would ordinarily be ample time for a relatively small volume of added water to redistribute such that the measured water content profiles should reflect natural sediment textural variations that are influenced primarily by ambient recharge conditions. However, given the caustic nature of the leaked fluids (to be discussed in Section 3) and the evidence for thermally enhanced moisture redistribution, the water content distributions were likely also influenced to some extent by other factors in addition to heterogeneity.

The volumetric water content values for all measurement locations in the two deeper access pipes are shown in Figure 2.8. Again, the extent to which the variability in water content in these two deeper access pipes might have been influenced by the B-Cell leak is difficult to determine. At their entry points, these deeper access pipes are offset by about 10 m from the horizontal access pipes. If the leak volume from B-Cell was relatively small, then the variability in the water content profiles shown for these two

deeper access pipes should reflect primarily the heterogeneity of the sediments under ambient groundwater recharge conditions from natural precipitation (albeit as affected by surface structures).

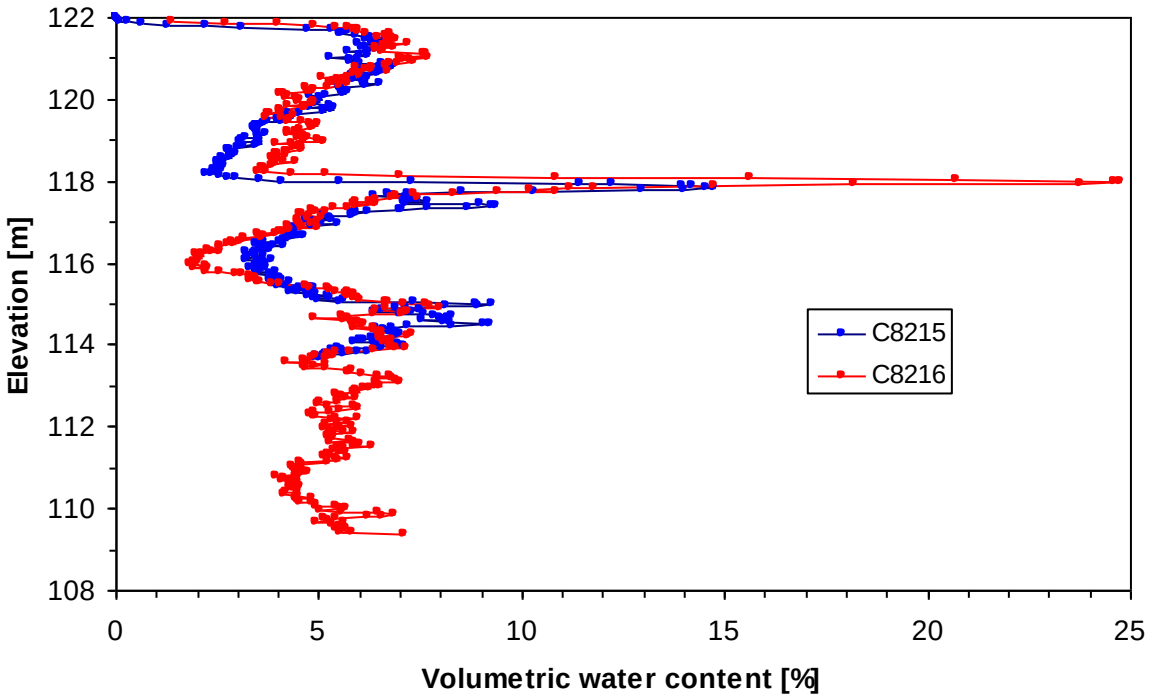

Figure 2.8. Volumetric water content values measured in two deeper angle-drilled access pipes.

The character of the water content profiles in Figure 2.8 is typical of a repeating sequence of fining-upward sediments. The smallest water content values, located at elevations of approximately 116 m and just above 118 m, are likely from coarser-textured sediments with lower water-holding capacity. Water content grows larger with increasing elevation above these locations, suggesting progressively increasing mass fractions of finer-grained sediment. This configuration is consistent with the depositional environment in which these sediments were deposited (Bjornstad et al. 2009). Unfortunately, no physical samples were collected from the closed-end steel access pipes, so the actual properties of the sediments at these locations have not been directly determined.

The significantly larger water content values shown in Figure 2.8 at an elevation of approximately 118 m clearly mark the position of a relatively sharp textural contrast. The spike in water content is likely silt or fine sand that is overlain by coarse sand or gravel. This behavior can also be caused by the so-called capillary barrier effect, in which finer-grained sediment overlies coarser-grained sediment and the entry pressure of the coarser sediment must be overcome before water will enter it. Until that point, infiltrating water will accumulate and be diverted laterally in the overlying finer-grained sediment. Note that regions of higher and lower water content can also be seen as the darker and lighter areas, respectively, on the sides of the pit shown in Figure 1.2.

Measured volumetric water content data are shown with calculated activity values for four of the horizontal access pipes in Figure 2.9. Activities were calculated from exposure rate measurements using

the MCNP code.[1] There is an inverse correlation between calculated activity values and volumetric water content data for the higher elevations (shallower depths).

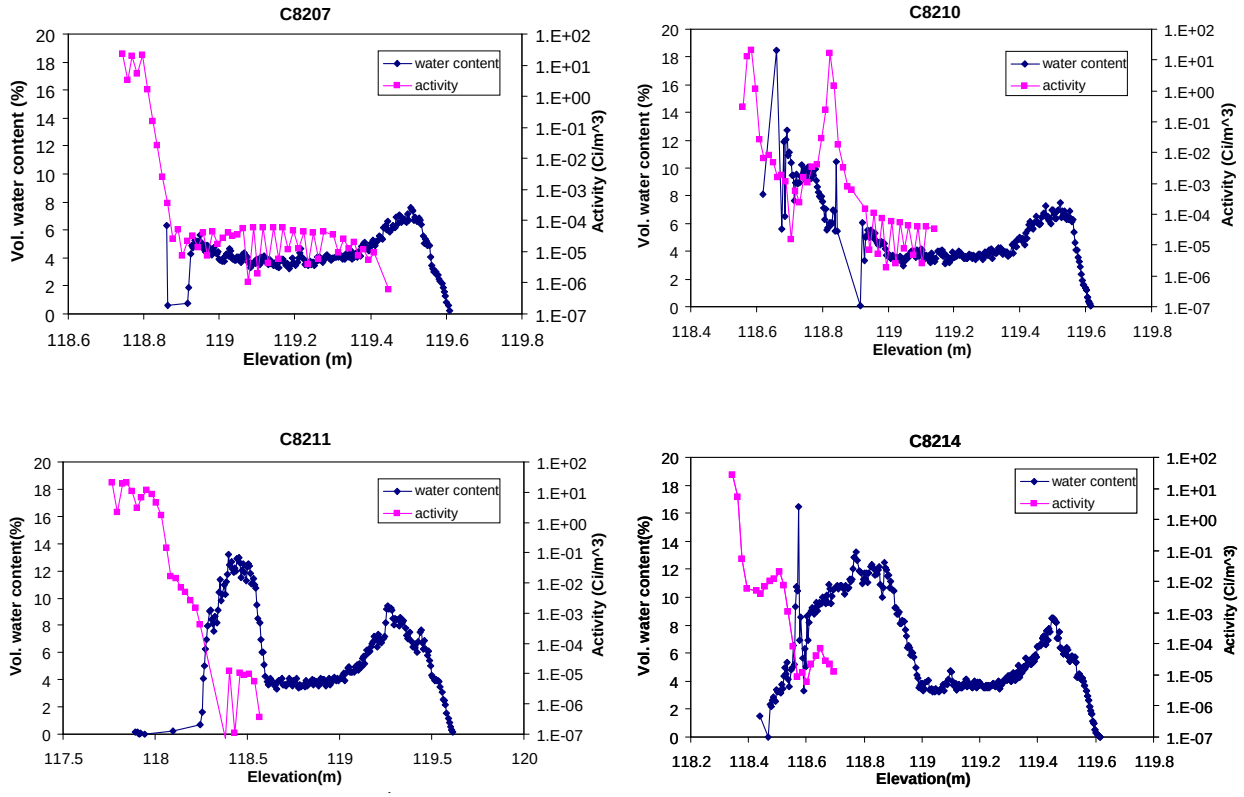

Figure 2.9. Measured volumetric water content data and calculated activities under B-Cell for four near-horizontal access pipes. The calculated activities correspond to the low-density case reported by WCH.

This apparent correlation is consistent with the interpretation that decay heat has created dried-out regions in some areas and increased water content in other areas due to thermally enhanced moisture redistribution.

WCH used the calculated total activities from MCNP modeling of the exposure rate data in conjunction with the ratio of the estimated activities of ^{137}Cs and ^{90}Sr reported for the B-Cell leak to estimate the spatial distributions of activity for each of these two species.[1] There are several complications with this type of calculation. The exposure rate data are not selective in distinguishing between ^{137}Cs, which emits gamma radiation, and ^{90}Sr, which emits beta radiation. However, steel blocks beta radiation, so the Geiger-Müller (GM) -based exposure rate meters should not have directly measured the primary beta emissions emanating from ^{90}Sr in the sediment surrounding the steel access pipes. On the other hand, Brehmsstrahlung radiation associated with ^{90}Sr decay could penetrate and accumulate within the steel access pipes and then be detected by the GM counter. In contrast, gamma radiation emitted by ^{137}Cs in the immediate vicinity of the access pipes would not be significantly shielded by steel

[1] WCH, 2011, Characterization of the Soil Contamination Under 324 B Cell, Calculation No. 0300X-CA-N0140, Rev. 1., Washington Closure Hanford, Richland, Washington; unpublished data.

and should therefore have been directly detected. ^{137}Cs and ^{90}Sr also have different sorption behavior. ^{137}Cs would likely have been preferentially adsorbed and concentrated at shallower depths relative to ^{90}Sr. For these reasons, the calculated ^{137}Cs and ^{90}Sr activities based on MCNP modeling have not been used for any quantitative calculations in this report. At present, simulated activities from flow and transport modeling have been compared with only measured activities from actual physical samples (Section 3).

2.3 Measured ^{137}Cs and ^{90}Sr Activities for Two Sediment Samples Collected under the B-Cell

To date, only two sediment samples have been collected from under the B-Cell for direct measurement of ^{137}Cs and ^{90}Sr activities and other geochemical properties. Two open-end steel access pipes were installed to collect these two sediment samples from under the B-Cell. The target sampling locations were two depths, approximately 4 ft apart, located directly above and below each other under the B-Cell sump where the highest activities were expected. The actual sampled locations are known only approximately, based on the starting coordinates and angles of the access pipes and the total pipe length (MW Perrott, WHC, personal communication, August 2011). No gyroscope surveys were conducted in the open-end access tubes used for obtaining the physical samples to verify final positions, in order to prevent contamination of expensive equipment. Therefore, there is some uncertainty in the locations of the actual sample points. Table 2.1 lists the measured activities of ^{137}Cs and ^{90}Sr and the calculated coordinates for the two sediment samples. These data are compared with simulation results in Section 3.

Table 2.1. Calculated spatial coordinates and measured ^{137}Cs and ^{90}Sr activities for two physical samples collected from under the B-Cell sump. (Coordinates are referenced to Washington State Plane South – NAD83, and NAVD88.)

Sample Coordinates						Measured Activities	
Easting(ft)	Northing(ft)	Elev.(ft)	Easting(m)	Northing(m)	Elev.(m)	^{137}Cs [μCi/g]	^{90}Sr [μCi/g]
1949634.14	379917.64	390.83	594248.49	115798.90	119.12	7985	377.5
1949634.14	379917.64	386.83	594248.49	115798.90	117.91	4.43	291.5

Source: PNNL, 2011, Transmittal of Analytical Data Reports in Support of 324 Soils Analysis, CCN # 161417, Pacific Northwest National Laboratory, Richland, Washington.

2.4 Measured Physical and Hydraulic Properties and Cation Exchange Capacity for Two Sediment Samples Collected from a Pit Excavated on the North Side of the 324 Building

Modeling of subsurface flow and transport processes requires a number of parameters that must be determined either experimentally, using site-specific data, or from previously measured data and parameters representing similar materials. Collection of core samples by drilling under the 324 Building was not considered to be feasible because of concerns about subsurface contamination and risk to workers. Prior to collection of the neutron-moisture data, the sediment profile underlying the 324 Building was conceptualized as a two-layer system consisting of a relatively thin and uniform sand

layer overlying a thicker gravel layer (see Figure 1.2). Therefore, two bucket samples of clean sediments were collected from the pit that was excavated on the north side of the 324 Building. One sample was collected from a part of the sediment profile representing the sand layer, and one sample was collected from the underlying gravel-dominated layer. Photographs of these sediment samples are shown in Figure 2.10.

Figure 2.10. Sand- and gravel-dominated sediments collected from a pit excavated on the north side of the 324 Building.

2.4.1 Grain-Size Distributions

Grain-size distributions were measured for subsamples of these two sediment types by both PNNL and by Shaw Environmental (Shaw 2011) using sieve and hydrometer methods (Gee and Or 2002). Data generated by PNNL and Shaw are plotted together in Figure 2.11. The gravel-dominated sediment has a coarser overall texture and is more poorly sorted, with a bimodal distribution of grain sizes. This gravel-dominated sediment also contains a larger mass fraction of silt- and clay-sized particles compared to the sand-dominated sediment and is classified as *muddy sandy gravel* (msG) using the Folk–Wentworth textural classification scheme (Folk 1980). The sand-dominated sediment is classified simply as *sand*.

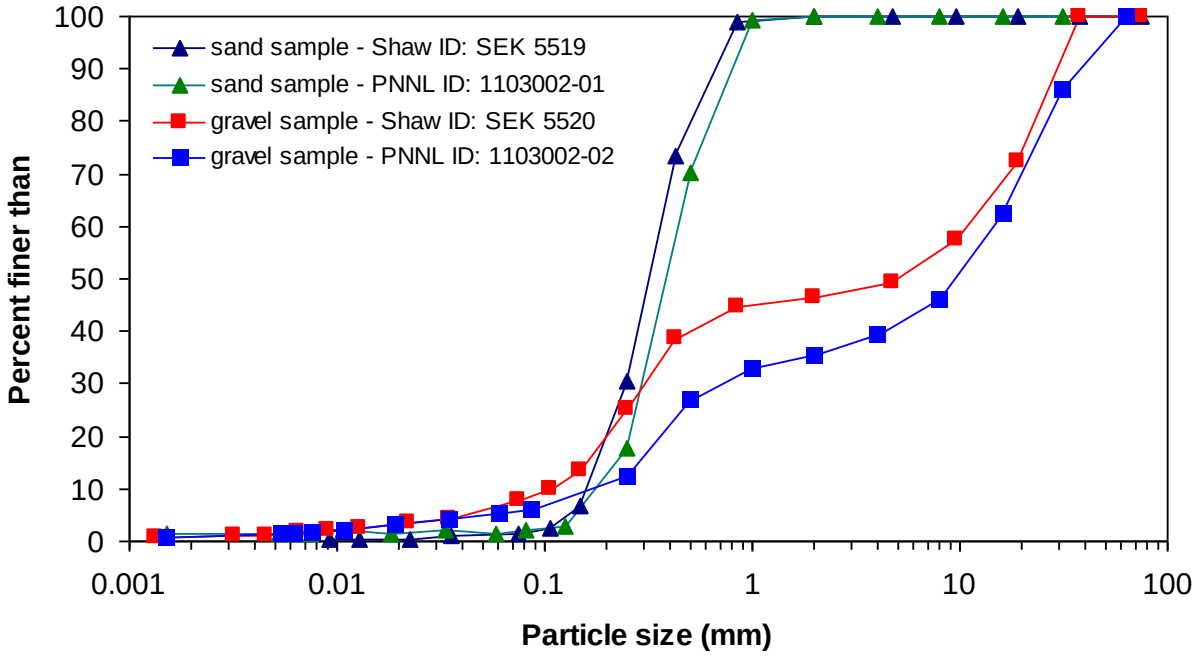

Figure 2.11. Cumulative grain-size distribution data for subsamples of the sand and gravel-dominated sediments collected from the pit that was excavated on the north side of the 324 Building. Data were generated by both PNNL and Shaw Environmental using sieve and hydrometer methods.

2.4.2 Hydraulic Properties

Subsamples of the sand and msG sediments were also packed into columns for measurement of saturated hydraulic conductivity. PNNL and Shaw used the falling head and constant head methods, respectively, for measurement of saturated hydraulic conductivity (Reynolds et al. 2002). PNNL also used the same repacked samples in the same sample holders for measurement of water retention characteristics using the hanging water column method (Dane and Hopmans 2002). Shaw used a chilled mirror hygrometer method to measure water retention characteristics in the vapor adsorption range of soil-moisture tension. The water retention data generated by PNNL and Shaw were initially combined and fit to estimate water retention parameters.

Water retention data, saturated hydraulic conductivities generated by PNNL, and fitted parameters for the van Genuchten (1980) water retention and Mualem (1976) hydraulic conductivity models are shown

in Figure 2.12. Preliminary simulation results yielded water content values that were too low, relative to the values measured by neutron logging in the field. Therefore, selected water retention data were refit to increase the residual water content, θ_r. The refit results are shown in the bottom panels of Figure 2.12.

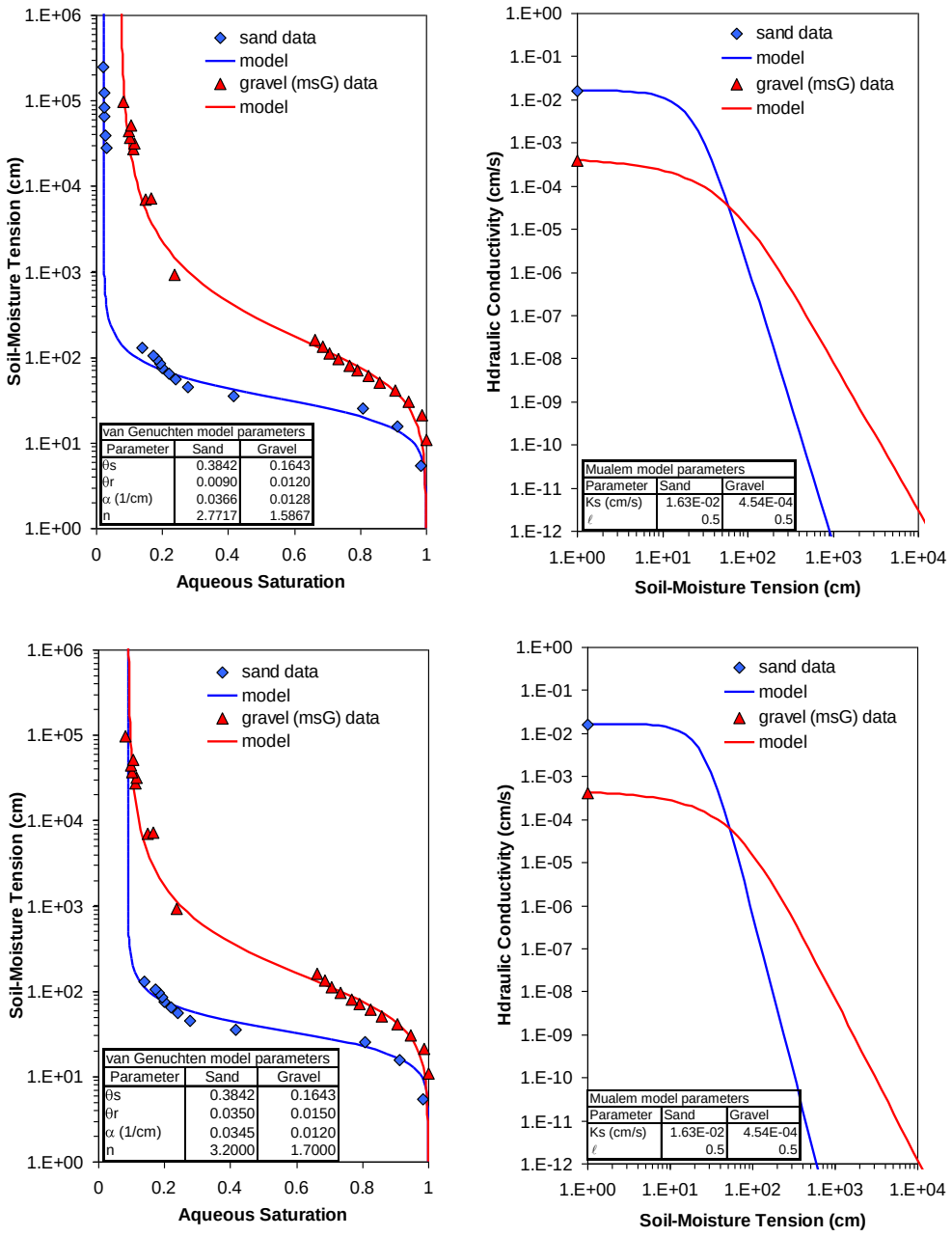

Figure 2.12. Water retention and hydraulic conductivity data with fitted parameters for the van Genuchten (1980) model. Bottom panels show results of refitting selected data to increase the residual water content.

Although the fits to the data shown in Figure 2.12 are relatively good, selected data were also refit using the Brooks and Corey (1964) water retention model. These results are shown with the fitted model parameters in Figure 2.13. The fits shown in Figure 2.13 are not as good as those shown in Figure 2.12.

However the Brooks–Corey model uses a distinct air-entry pressure (h_b) that will frequently yield flow and transport simulation results that better match field observations in sediments that have sharp interfaces between sediment types with large contrasts in texture. The spike in water contents at the ~118-m elevation shown previously in Figure 2.8 suggests that there is at least one such sharp interface underlying the B-Cell.

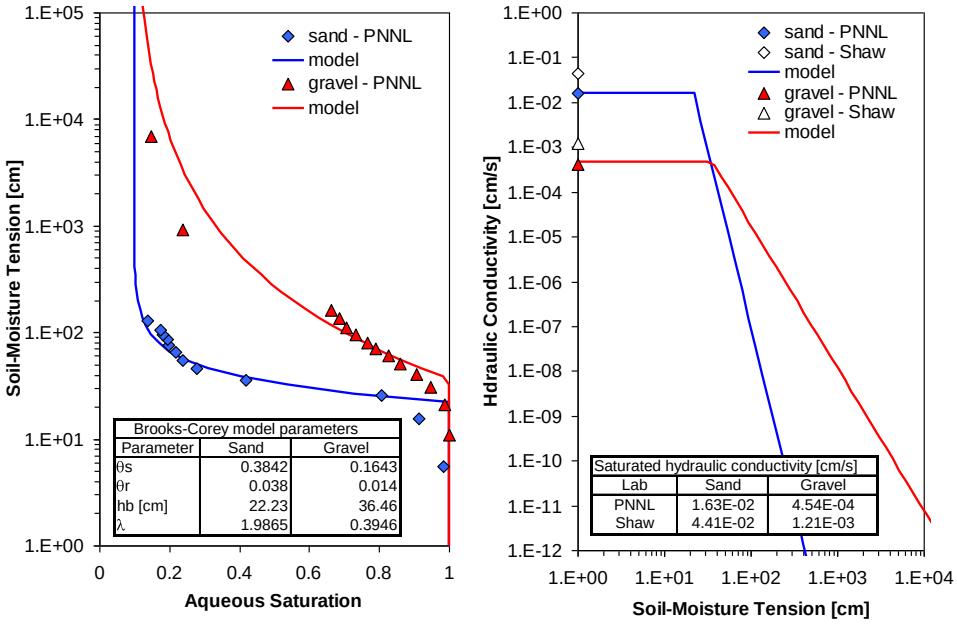

Figure 2.13. Water retention and saturated hydraulic conductivity data and Brooks–Corey model parameters. Unsaturated hydraulic conductivity calculated using Burdine (1953) model.

The hydraulic conductivity plot shown in Figure 2.13 also shows and lists the saturated hydraulic conductivity values (K_s) determined by both PNNL and Shaw for subsamples of these sediments. The K_s values determined by PNNL and Shaw for the sand are 1.63×10^{-2} cm/s and 4.41×10^{-2} cm/s, respectively; the Shaw result is a factor of 2.7 greater than the PNNL result. The K_s values determined by PNNL and by Shaw for the gravel (msG) are 4.54×10^{-4} cm/s and 1.21×10^{-3} cm/s, respectively; the Shaw result is a factor of 2.5 greater than the PNNL result. As noted previously, different methods were used for estimating K_s, so these differences in values produced by PNNL and Shaw could be attributed in part to that factor. However, as shown in Figure 2.11, the grain-size distributions of the subsamples used by PNNL and Shaw were not exactly the same, and these sediments were likely packed differently by the two laboratories. Both the PNNL water retention and K_s measurements were performed on the same cores of repacked sediments. For this reason, the PNNL K_s values were used for flow and transport modeling. The Brooks–Corey model parameters shown in Figure 2.13 were also used in the model simulations because they yielded slightly better correspondence between simulated and observed water contents.

2.4.3 Cation-Exchange Capacity

Both ^{137}Cs and ^{90}Sr are cationic species known to adsorb to Hanford sediments. Therefore, reactive transport modeling was performed using a reaction network that includes the process of ion exchange.

This requires estimates of cation-exchange capacity (CEC), so these measurements were made on subsamples of the sand and gravel sediments. Table 2.2 lists CEC values that were determined by Shaw (Shaw 2001) and PNNL (see Appendix) on these two subsamples. Estimates of CEC determined by Zachara et al. (2002) on near-surface sediments from the vicinity of the Hanford S-SX tank farm are also shown in Table 2.2 for comparison.

Table 2.2. Cation-exchange capacity of sediment samples collected from the pit on the north side of 324 Building and from another Hanford Site sediment.

Description	CEC [meq Na^+/100 g](st dev, n)	Electrolyte	Laboratory (reference or procedure)
Sand	4.22 (0.04, 2)	--	Shaw (EPA, SW-846 9081)
Muddy sandy gravel	6.67	--	Shaw (EPA, SW-846 9081)
Sand	11.33 (0.11, 4)	--	PNNL[(a)] (Valenta 2008)
Muddy sandy gravel	14.75 (0.35, 4)	--	PNNL (Valenta 2008)
Sandy silt	4.26 (0.12, 6)	Na^+	Zachara et al. 2002
Sandy silt	8.25 (0.35, 6)	K^+	Zachara et al. 2002
Sandy silt	4.69 (0.14, 6)	Ca^{2+}	Zachara et al. 2002

(a) The PNNL procedure does not include NaOAc pretreatment steps used in the EPA procedure.

The Na-equivalent CEC value estimated by Shaw for the sand (4.22 meq/100 g) is very similar to that estimated by Zachara et al. (2002) for a sandy silt sediment (4.26 meq/100 g) from the Hanford S-SX tank farm area. In contrast, the CEC values estimated by PNNL are factors of approximately 2.7 and 2.2 greater than those estimated by Shaw for the sand and muddy sandy gravel sediments, respectively. Although there are some differences in the sediment subsamples that were used by Shaw and by PNNL (Figure 2.11), the differences in CEC values appear to be primarily a result of different laboratory methods and sediment pretreatment steps. The EPA-based CEC measurement procedure used by Shaw (EPA 1986) uses repeated sodium acetate (NaOAc) pretreatment steps, followed by multiple isopropyl alcohol rinse steps, followed by multiple rinses with ammonium acetate (NH_4OAc) solution prior to final measurement of Na^+ concentration in the supernatant for determination of CEC. Zachara et al. (2002) states that the CEC values reported in their study were also determined on NaOAc-treated sediments (Babcock and Schulz 1970). The PNNL procedure described by Valenta (2008) does not use NaOAc pretreatment or isopropyl alcohol rinse steps. For sediments with high concentrations of salts, the PNNL procedure calls for multiple pre-rinse steps with double de-ionized water, but no pretreatment steps were performed on the 324 Building pit samples. Given the lack of sediment pretreatment steps, the higher apparent CEC values generated using the PNNL procedure are likely a result of calcite dissolution. The pretreatment steps in the EPA procedure used by Shaw would tend to dissolve calcite and to remove any exchangeable or calcite-associated Ca^{2+} prior to the CEC measurement. Therefore, the CEC values determined by Shaw were deemed to be more representative and were used for the reactive transport modeling described in Section 3.

3.0 Flow and Transport Modeling

Numerical modeling of the B-Cell spill was a multistep process consisting of geochemical modeling, 1-D flow and reactive transport modeling, and 3-D flow and solute transport modeling. The following sections describe these steps.

Water flow and solute transport modeling was performed using the water operational mode of the Subsurface Transport Over Multiple Phases (STOMP) simulator (White and Oostrom 2006). This operational mode solves a mass balance equation for water under isothermal, single (aqueous)-phase conditions, and an additional mass balance equation for each transported solute or radioactive species. The basic flow and solute transport modeling capabilities in this mode of STOMP have been tested and qualified for use in regulatory-related calculations. Reactive transport modeling, involving aqueous speciation, ion-exchange, and precipitation-dissolution reactions, was also performed using the ECKEChem module of STOMP (White and McGrail 2005).

It should also be noted that the temperature measurements and computed activities based on the dose rate measurements from under the B-Cell indicate that the heat of radioactive decay has generated non-isothermal and multiphase flow conditions (thermally enhanced moisture redistribution in both aqueous and gas phases) under the 324 Building. Although there is a water–air–energy operational mode of STOMP that solves the coupled energy and mass balance equations that would be needed to accurately model this system, this mode does not currently account for heat generation by radioactive decay. Consequently the modeling results presented here, generated using the water operational mode of STOMP, do not fully account for all of the processes that have affected the observed field measurements.

3.1 Geochemical Modeling

Geochemical modeling was performed to estimate the composition of the initial aqueous solution that was spilled in B-Cell and its changes after reaction with the concrete foundation of the building. All geochemical modeling was performed using EQ3/6 Version 8 (Wolery and Jarek 2003).

3.1.1 Estimation of Initial Spill Composition

The exact chemical composition and volume of waste that was spilled in the B-Cell of the 324 Building is unknown. The only known release of sufficient magnitude to yield the dose rates that have been measured under the building was a single spill of concentrated radioactive liquid associated with a Federal Republic of Germany (FRG) Canister Fabrication Project, known locally as the FRG glass log project.[1]

Historical records provided to PNNL by WCH indicate that the concentrated waste streams that were being used in the FRG project had the nominal compositions shown in Table 3.1. Records also indicate that the processing operations at that time involved blending the waste streams with glass-forming chemicals and then using a formic acid (26M) denitrification process for further treatment of the wastes. However, records were insufficient for determining what stage of processing was being performed or the

[1] WCH, 2011, Characterization of the Soil Contamination Under 324 B Cell, Calculation No. 0300X-CA-N0140, Rev. 1., Washington Closure Hanford, Richland, Washington.

exact composition of the waste that was actually spilled in B-Cell. Therefore, the waste was assumed to have the nominal composition shown in Table 3.1.

Table 3.1. Reported compositions of concentrated waste streams used in FRG canister fabrication project (anion composition not reported).[(a)]

Element	Cesium Waste Stream Composition, mole/L	Strontium Waste Stream Composition, mole/L
Ag	0.00019	--
Al	--	0.00958
Ba	0.00159	0.00831
Ca	0.00323	0.0496
Cd	--	0.0065
Ce	--	0.0008
Cr	0.00149	0.00639
Cs	0.137	0.00156
Cu	0.00015	--
Fe	0.00862	0.0351
La	0.000727	0.0292
Mg	0.00179	0.0124
Mn	--	0.00953
Na	0.124	0.5
Ni	0.00225	--
Nd	--	0.0065
Pb	--	0.0023
Si	0.00466	--
Sr	0.00158	0.113
H^+ (M)	3.5	3.3
^{90}Sr (Ci/L)	--	475
^{137}Cs (Ci/L)	460	6

(a) "FRG Canister Fabrication." Presentation dating from the 1980s, author anonymous. Document Control No 164372, Washington Closure Hanford LLC, Richland, Washington; unpublished.

Modeling of the B-Cell leak chemistry was done in stages using EQ3/6. First, using EQ3, a 50:50 mixture of the cesium and strontium waste streams shown in Table 3.1 was equilibrated using NO_3^- for charge balance. Second, using EQ6, the mixture was concentrated so that 510 L of the mixed waste stream water yielded a radioactivity of 1.3 million curies, which was the estimated total activity of the spill. Assuming an equal volume mix of the cesium and strontium waste streams and charge balancing the solution on nitrate using EQ3 gives the composition shown in Table 3.2. The calculated pH of this mixed waste concentrate is −1.14. This extremely acidic solution would have reacted with the concrete in the B-Cell floor. Photographs (not shown) of the stainless steel sink and drain in B-Cell showed them to be highly corroded, which corroborates the assumption that at least some of the waste solutions being used in B-Cell were either acidic or caustic.

3.1.2 Estimation of Spill Composition after Reaction with Concrete

To account for the buffering of the acidic waste solution by the concrete foundation prior to entering the sediment profile under the 324 Building, the EQ6 code was used to react the waste mixture with concrete. It was assumed that the FRG canister waste concentrate reacted with Portland cement for 1 day. The Portland cement was represented by the minerals sodium hydroxide, portlandite, ettringite, and tobermorite-14A. A low specific surface area of 4.17e-3 cm^2/g was used for the concrete components because it was assumed that the concentrate did not actually seep into the concrete but contacted only the surface. Table 3.3 shows the spill composition after reaction with concrete. After reaction with concrete, the simulated pH value increased to 1.29. Note the very high concentration of Ca^{2+} in Table 3.3 relative to the concentrations shown in Tables 3.1 and 3.2, which results from dissolution of the concrete minerals.

Table 3.2. Computed species concentrations of mixed waste stream.

Species	Molarity
Ag+	4.66E−04
Al+++	2.35E−02
Ba++	2.43E−02
Ca++	1.30E−01
Cd++	1.60E−02
Ce+++	1.96E−03
CrO4−−	1.93E−02
Cs+	3.40E−01
Cu++	3.68E−04
Fe++	1.07E−01
H+	1.67E+01
HCO3−	1.05E−06
K+	4.91E−15
La+++	7.35E−02
Mg++	3.48E−02
Mn++	2.34E−02
NO3−	2.01E+01
Na+	1.53E+00
Nd+++	1.60E−02
Ni++	5.52E−03
Pb++	5.65E−03
SO4−−	4.91E−15
SiO2(aq)	6.66E−04
Sr++	2.81E−01

Table 3.3. Computed spill composition after reaction with concrete.

Species	Molarity
Al+++	1.04E+00
Ba++	2.71E−04
Ca++	3.38E+00
CrO4−−	1.10E−02
Fe++	8.41E−05
H+	2.92E−03
HCO3−	6.48E−07
K+	2.80E−15
La+++	4.20E−02
Mg++	1.99E−02
Mn++	1.34E−02
NO3−	1.15E+01
Na+	8.92E−01
SO4−−	8.38E−03
SiO2(aq)	6.66E−04
Sr++	1.61E−01
Cs+	1.94E−01

The spill is also described as follows:[1]

> During routine transfers of radioactive material on October 21, 1986 for the FRG Canister Fabrication Project, approximately 510 liters of concentrated $^{137}Cs/^{90}Sr$ solution leaked to the floor of B-Cell. The estimated radiochemical inventory of the solution was 883 kCi of ^{137}Cs and 388 kCi ^{90}Sr.

The difference between the Cs/Sr ratio cited by WCH and that shown in Table 3.1 suggests that the concentrated waste streams may have been blended in different proportions. However, it is not known with certainty whether the material that was actually spilled was a blend of these concentrated waste streams or if the spilled fluids were in some stage of mixing with other glass-forming chemicals, or if they were spilled during the formic acid denitrification process.

For reactive transport modeling, the post-concrete EQ3/6 equilibrated concentrations shown in Table 3.3 were used to represent the initial concentrations of all species shown, except for Sr++, Cs+, and Ca++, whose concentrations were adjusted as follows. The estimated total activities of 883 kCi ^{137}Cs and 388 kCi ^{90}Sr correspond, with total masses of 2.834 kg ^{90}Sr and 10.157 kg ^{137}Cs, respectively. Assuming these total masses are mixed with specific volumes of water (e.g., 25, 50, or 100 gal) and combining the ^{90}Sr and ^{137}Cs concentration values estimated in this way with the other species concentrations shown in Table 3.3, excluding Ca2+, and then charge balancing on Ca2+ yields alternative suites of potential spill compositions. Table 3.4 shows the calculated post-concrete reacted spill compositions that were

[1] WCH, 2011, Characterization of the Soil Contamination Under 324 B Cell, Calculation No. 0300X-CA-N0140, Rev. 1., Washington Closure Hanford, Richland, Washington.

estimated in this way for three dilution volumes. The spill compositions and volumes shown in Table 3.4 were used for reactive transport modeling.

Table 3.4. Changes in species concentrations (relative to Table 3.3) resulting from application of different mixing volumes to the Sr2+ and Cs+ masses that correspond to total activities of 883 kCi and 388 kCi, respectively, with charge balance on Ca2+. Yellow highlighted entries indicate species whose concentrations were varied for different simulation cases.

		Dilution Volume					
		25 gal		50 gal		100 gal	
Species	Charge	M	Equivalent	M	Equivalent	M	Equivalent
Al+++	3	1.04E+00	3.12E+00	1.04E+00	3.12E+00	1.04E+00	3.12E+00
Ba++	2	2.71E−04	5.42E−04	2.71E−04	5.42E−04	2.71E−04	5.42E−04
Ca++	2	2.94E+00	5.88E+00	3.30E+00	6.61E+00	3.48E+00	6.97E+00
CrO4−−	−2	1.10E−02	−2.20E−02	1.10E−02	−2.20E−02	1.10E−02	−2.20E−02
Fe++	2	8.41E−05	1.68E−04	8.41E−05	1.68E−04	8.41E−05	1.68E−04
H+	1	2.92E−03	2.92E−03	2.92E−03	2.92E−03	2.92E−03	2.92E−03
HCO3−	−1	6.48E−07	−6.48E−07	6.48E−07	−6.48E−07	6.48E−07	−6.48E−07
K+	1	2.80E−15	2.80E−15	2.80E−15	2.80E−15	2.80E−15	2.80E−15
La+++	3	4.20E−02	1.26E−01	4.20E−02	1.26E−01	4.20E−02	1.26E−01
Mg++	2	1.99E−02	3.98E−02	1.99E−02	3.98E−02	1.99E−02	3.98E−02
Mn++	2	1.34E−02	2.68E−02	1.34E−02	2.68E−02	1.34E−02	2.68E−02
NO3−	−1	1.15E+01	−1.15E+01	1.15E+01	−1.15E+01	1.15E+01	−1.15E+01
Na+	1	8.92E−01	8.92E−01	8.92E−01	8.92E−01	8.92E−01	8.92E−01
SO4−−	−2	8.38E−03	−1.68E−02	8.38E−03	−1.68E−02	8.38E−03	−1.68E−02
SiO2(aq)	0	6.66E−04	0.00E+00	6.66E−04	0.00E+00	6.66E−04	0.00E+00
Sr++	2	3.33E−01	6.66E−01	1.66E−01	3.33E−01	8.32E−02	1.66E−01
Cs+	1	7.83E−01	7.83E−01	3.92E−01	3.92E−01	1.96E−01	1.96E−01
		Sum:	1.00E−08	Sum:	−6.11E−16	Sum:	8.05E−16

3.2 One-Dimensional Flow and Reactive Transport Modeling

All flow and transport modeling was performed using the STOMP simulator (White and Oostrom 2006). A one-dimensional, vertically oriented variably saturated flow and reactive transport model was first developed to generate initial estimates of flow and transport behavior for comparing with field observations. The cross-sectional area (*x*–*y* plane) of the one-dimensional (1-D) model is 0.25 m^2 (0.5 m × 0.5 m), which is the same *x*–*y* dimension of the grid blocks used as sources in the three-dimensional (3-D) model, to be described in more detail later.

The 3-D model has 50 cells, each 0.5 m × 0.5 m in the *x*–*y* plane, in which source terms were used to represent a distributed leak aligned in a rectangular pattern. This pattern coincides approximately with the plan-view outline of the expansion joints in the concrete foundation of the B-Cell pad through which the leak was presumed to have emanated.

Uniform 0.25-m grid spacing was used in the vertical direction for the 1-D model. Upper boundary conditions were specified water fluxes and specified concentrations. Lower boundary conditions were specified water pressure (water table condition) and outflow boundary conditions for the aqueous species.

Reactive transport modeling requires the development and parameterization of a reaction network. The following types of reactions were considered: ion exchange, aqueous speciation, mineral precipitation, and dissolution. Details regarding each type of reaction and parameters are provided in the following sections, followed by simulation results.

3.2.1 Ion-Exchange Reactions

Both ^{90}Sr and ^{137}Cs are cations known to adsorb strongly to Hanford sediments under most conditions (Cantrell et al. 2007; Last et al. 2006). According to Stumm and Morgan (1996), for most clays and oxide surfaces, the following order of sorption affinity is usually observed:

$$Cs+ > K+ > Na+ > Li + Ba2+ > Sr2+ > Ca2+ > Mg2+ \quad (3.1)$$

with sorption affinity increasing with the (nonhydrated) radius of the ions. Although Equation (3.1) provides a rule of thumb for relative sorption affinity, a reversed selectivity may be observed for some zeolites and some glasses (Stumm and Morgan 1996).

At low pH conditions, the hydrogen ion can actually compete directly for exchange sites with Cs^+ (Poinssot et al. 1999) and Sr^{2+}. In fact, acid extraction has been used to remove ^{90}Sr for measurement (McKinley et al. 2007). Sorption coefficients have not been found in the literature for pH values as low as what was calculated for the assumed FRG canister waste chemistry, although experimental data do show a marked decrease in cesium and strontium sorption on clays at pH values between 2 and 3 (Papelis and Um 2003). Experiments with sorption of strontium on magnetite also show that at acidic pH, sorption can be negligible.

Geochemical conditions are expected to have evolved significantly from the time the FRG canister wastes were first spilled to the time when concentrations were measured in the subsurface, some 25 years later. Specifically, the initially acidic waste entering the subsurface would likely have been buffered further by the sediments. To address the potential evolution of this geochemical system, a reaction network was developed that includes the processes of ion-exchange, aqueous-speciation, and mineral precipitation/dissolution reactions.

Modeling of ion-exchange processes requires estimates of CEC and selectivity coefficients (Valocchi et al. 1981; Sposito 1994; Appelo et al. 1994), as well as measurements of aqueous solution chemistry. CEC measurements are discussed in Section 2. Selectivity coefficients, which are essentially mass law constants for describing equilibria for the exchange of ions, are usually determined experimentally for a given set of chemical conditions. Selectivity coefficients were not directly measured for this study, but a number of other studies have been performed with Hanford sediments to determine selectivity coefficients for exchange reactions involving Sr^{2+} and Cs^+. For example, McKinley et al. (2007) reported selectivity coefficients for exchange reactions involving Sr^{2+} that were estimated by fitting experimental data (Lichtner and Zachara 2005). Zachara et al. (2002) and Liu et al. (2004) developed different models and associated parameters describing Cs^+ sorption in Hanford sediments. The models developed by Zachara and co-workers typically consider multiple types of exchange sites (e.g., frayed edge and planar

surface sites) that have different sorption affinities (strong and weak). Liu et al. (2004) demonstrated that Cs^+ selectivity coefficients for Hanford sediments are dependent on electrolyte concentrations, with log selectivity coefficients generally increasing with increasing electrolyte concentration.

The STOMP simulator that was used for flow and transport modeling in this study currently considers only one type of sorption site for exchange reactions and uses constant values for the selectivity coefficients. It also uses the Gaines–Thomas activity convention for exchange reactions (Gaines and Thomas 1953). Other conventions such as the Vanselow activity convention (Sposito 1994) have been used in some of the previous Hanford studies (Liu et al. 2004). The initial spill in the B-Cell appeared to have been highly concentrated and very acidic. However, the initial spill was diluted by an unknown volume of rinse water with unknown composition. The acidity was also buffered by reactions with the concrete foundation of the building and the underlying sediments. Based on these considerations, an intermediate value between the strong (K_v^I) and weak (K_v^{II}) sorption site selectivity coefficients reported by Liu et al. (2004) was used to represent Cs–Na exchange. The selectivity coefficients reported by McKinley et al. (2007) were used to represent Sr^{2+} and exchange reactions for other major cations. These parameters are summarized in Section 3.2.3 of this report.

3.2.2 Aqueous Speciation and Mineral Reactions

Aqueous speciation and mineral precipitation/dissolution reactions were also considered, based on the composition of the FRG glass waste simulant and speciation calculations performed with EQ3/6. Selected mineral species and their average volume fractions for the sediments underlying the 324 Building were based on unpublished data (JP McKinley, PNNL, private communication, March 2011) for sediments from the DOE Office of Science IFRC site, located approximately 200 m north of the 324 Building (see Figure 1.1). The bulk mineralogy of the sand and gravel were assumed to be the same, and are based on average values for Hanford formation sediments at the IFRC site, shown in Table 3.5.

Table 3.5. Average mineral composition of Hanford formation sediments at the IFRC site, 300 Area.

Hanford Formation Sediment	Average Mineral Composition (vol%)
Quartz	18.9
Augite	10.3
Montmorillonite	3.2
Chlinochlore	2.9
Muscovite	16.7
Feldspar	48.2
Total	**100.0**

The mineral augite listed in Table 3.5 is not included in the EQ3/6 v8.0 database from which equilibrium and solubility product constants were obtained. Therefore, augite was replaced with an equal volume mixture of diopside (5.15%) and hedenbergite (5.15%) for the reactive transport simulations. A small amount of calcite (0.01%–0.02%) was also added, based on the results of the CEC measurements. The temperature used for the STOMP reactive transport simulations was 25 °C. Reaction rates for soil

minerals were taken from a compilation by the U.S. Geological Survey (Palandri and Kharaka 2004). Table 3.6 shows the reactions, equilibrium constants, and references used for the full reaction network.

3.2.3 One-Dimensional Simulation Results

The results of three 1-D simulation cases are presented. These three simulation cases assume that the entire radionuclide inventory was contained in 25, 50, or 100 gal (Table 3.4), and that this entire inventory entered the subsurface during the course of 1 week. Thereafter, a constant rate of water release (25, 50, or 100 gal/wk) was assumed until 1992. After the initial 1-week leak period, during which the water was assumed to have the composition of the FRG waste stream, subsequent radionuclide-free water was introduced into the model with the chemical composition of Columbia River water (Ma et al. 2010). The actual water fluxes used for the 1-D model are 0.00108, 0.00216, and 0.00432 m/d, which correspond to 25, 50, and 100 gal/wk, respectively, in the 3-D model, divided over 50 cells of equal cross-sectional area. These constant water fluxes were applied over the time from the leak in 1986 to 1992. After 1992, it is assumed that grout, which was spilled into the B-Cell sump, prevented any additional water from entering the subsurface through the foundation under B-Cell. Simulations were continued from 1992 to 2012 but with no additional water added to the system.

Only two sediment samples were collected by WCH for chemical analyses from direct-push sampling beneath the B-Cell. The target sample locations were two depths, approximately 4 ft apart, directly beneath the B-Cell sump, where the highest radionuclide activities were expected. However, the actual sampled locations are known only approximately, based on the starting coordinates and angles of the Geoprobe pushes and the total pipe length (MW Perrott, WCH, private communication, August 2011). No gyroscope surveys were conducted in the open-end access tubes used for obtaining the physical samples, in order to prevent contamination of expensive equipment, so there is some uncertainty in the actual locations of the sample points.

Figure 3.1 shows the sample data at their calculated elevations and simulation results for ^{137}Cs and ^{90}Sr for the year 2011. Simulation results were generated using the full reaction network whose reactions, selectivity coefficients, and equilibrium constants are shown in Table 3.6. The three simulation cases were run using the assumed waste compositions shown in Table 3.4 and with the fluxes described above. Note that the reaction network used for these simulations did not account for the radioactive decay of ^{137}Cs and ^{90}Sr. Given the 1-D nature of these reactive transport simulations and the lack of accounting for radioactive decay, these results should yield conservative estimates of the contaminant concentrations and depth of migration, assuming that the simulated water release rates are similar to or greater than what actually occurred.

The separation of the simulated ^{137}Cs and ^{90}Sr profiles shown in Figure 3.1 is consistent with the selectivity coefficients that were specified for the exchange reactions. Although the simulation results are qualitatively similar to the observed data for the two sample points, the observed ^{90}Sr activities are over-predicted and the ^{137}Cs activities are under-predicted for the shallower of the two sampling locations. The observed activities for the deeper sampling location are bounded by the 25- and 50-gal/wk simulation cases. For ^{90}Sr, the higher leak rate of 100 gal/wk yields a simulated activity that is closer to the measured value for the shallow sampling depth.

Table 3.6. Reactions, selectivity coefficients, equilibrium constants (25 °C), and references.

	logK	Reference
Cation Exchange		
$2NaX + Sr^{2+} = SrX_2 + 2Na^+$	3.218	McKinley et al. (2007)
$2NaX + Ca^{2+} = CaX_2 + 2Na^+$	3.147	McKinley et al. (2007)
$2NaX + Mg^{2+} = MgX_2 + 2Na^+$	2.829	McKinley et al. (2007)
$NaX + K^+ = KX + Na^+$	1.322	McKinley et al. (2007)
$NaX + Cs^+ = CsX + Na^+$	4.630	Liu et al. (2004)[(a)]
Aqueous Speciation		
OH- = - H+	14.344	EQ3/6 database
AlOH++ = - H+ + Al+++	5.255	EQ3/6 database
AlSO4+ = Al+++ + SO4--	–3.010	EQ3/6 database
BaNO3+ = Ba++ + NO3-	–0.900	EQ3/6 database
CO3-- = - H+ + HCO3-	10.3288	EQ3/6 database
CaNO3+ = Ca++ + NO3-	–0.700	EQ3/6 database
CaSO4(aq) = Ca++ + SO4--	–2.087	EQ3/6 database
CaCO3(aq) = Ca++ + CO3--	–3.2	EQ3/6 database
Cr+++ = - 0.750O2(aq) + CrO4-- + 5H+	–13.832	EQ3/6 database
Cr2O7-- = 2CrO4-- + 2H+	–14.624	EQ3/6 database
Fe+++ = 0.250O2(aq) + Fe++ + H+	–5.557	EQ3/6 database
FeNO3++ = NO3- + 0.250O2(aq) + Fe++ + H+	–6.557	EQ3/6 database
H2CrO4(aq) = CrO4-- + 2H+	–4.924	EQ3/6 database
HCrO4- = CrO4-- + H+	–6.491	EQ3/6 database
HNO3(aq) = H+ + NO3-	1.399	EQ3/6 database
HSO4- = H+ + SO4--	–1.866	EQ3/6 database
La++ = - H+ - 0.250O2(aq) + La+++	–76.016	EQ3/6 database
MgSO4(aq) = Mg++ + SO4--	–2.299	EQ3/6 database
Mn(NO3)2(aq) = Mn++ + 2NO3-	–0.600	EQ3/6 database
MnNO3+ = Mn++ + NO3-	–0.200	EQ3/6 database
NaSO4- = Na+ + SO4--	–0.820	EQ3/6 database
SrNO3+ = NO3- + Sr++	–0.800	EQ3/6 database
SrCO3(aq) = CO3-- + Sr++	–2.81	EQ3/6 database
SrSO4(aq) = SO4-- + Sr++	–2.300	EQ3/6 database
Mineral Precipitation/Dissolution		
Alunite = - 6H+ + K+ + 2SO4-- + 3Al+++		EQ3/6 database
Anhydrite = Ca++ + SO4--		EQ3/6 database
Barite = Ba++ + SO4--		EQ3/6 database
Clinochlore-14A = - 16H+ + 2Al+++ + 3SiO2(aq) + 5Mg++		EQ3/6 database
Diaspore = - 3H+ + Al+++		EQ3/6 database
Diopside = - 4H+ + Ca++ + Mg++ + 2SiO2(aq)		EQ3/6 database
Hedenbergite = - 4H+ + Ca++ + Fe++ + 2SiO2(aq)		EQ3/6 database
Hematite = - 4H+ + 0.500O2(aq) + 2Fe++		EQ3/6 database
K-Feldspar = - 4H+ + Al+++ + K+ + 3SiO2(aq)		EQ3/6 database
Montmor-Ca = - 6H+ + 0.165Ca++ + 0.330Mg++ + 1.670Al+++ + 4SiO2(aq)		EQ3/6 database
Muscovite = - 10H+ + K+ + 3Al+++ + 3SiO2(aq)		EQ3/6 database
Quartz = SiO2(aq)		EQ3/6 database
Calcite = Ca++ + CO3--		EQ3/6 database

(a) Intermediate value of logK determined for strong and weak sites in a two-site model.

In addition to the factors noted previously, differences between observed and simulated results could be due to differences between the actual and simulated chemical compositions of the waste solution, water release rates and their distribution in time and space, selectivity coefficients, other physical and hydraulic properties (e.g., porosity, permeability, relative permeability–saturation–capillary pressure relations), and/or processes (e.g., thermal effects and two-phase flow) that were not addressed in the modeling. It is also possible that differences between observed and simulated activities could be due in part to physicochemical phenomena, such as competition for sorption sites/surface area between mineral reactions and exchange reactions and blocking of exchange sites by precipitated minerals. These latter effects are not accounted for in the reaction equations solved by STOMP. Finally, as suggested earlier, differences between observed and simulated activities could also be due, in part, to differences in the actual versus calculated locations of the physical samples because gyroscope surveys were not performed in the open-end access tubes to determine if their actual end points deviated from the target sampling locations. The exact locations/depths for the two physical samples are therefore uncertain. Based on these 1-D reactive transport modeling results, 3-D flow and transport modeling was performed, assuming water release rates of 50 and 100 gal/wk.

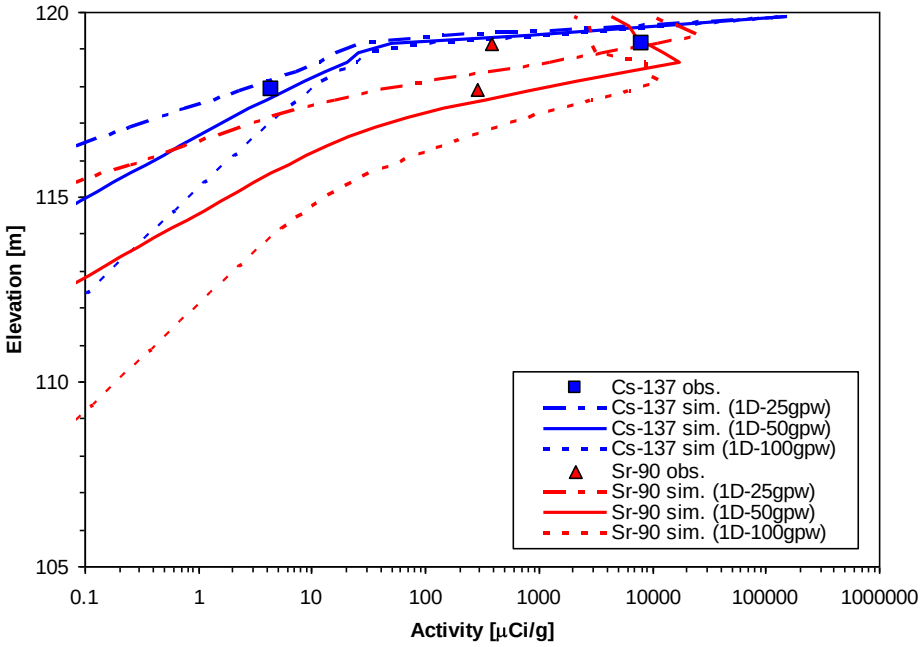

Figure 3.1. Observed ^{137}Cs and ^{90}Sr concentrations for two physical samples collected from under the B-Cell sump, and simulated concentrations 25 years after the spill (2011) generated from a 1-D reactive transport model using different water release rates.

Figure 3.2 shows simulated concentration profiles for the modeled exchangeable cations after 25 years. The CEC was initially assigned to the exchange species NaX. Sorbed Na^{+} was displaced by other exchangeable cations, including Sr^{2+} and Cs^{+}, during infiltration of the waste solution. Although Sr^{2+} was assigned a larger selectivity coefficient (logK value) than Ca^{2+}, the CaX2 concentrations are greater than SrX2 due to the much higher concentrations of Ca^{2+} in the simulated waste solution. CsX concentrations are shown to be much higher than SrX2 concentrations near the surface due to preferential adsorption resulting from the different selectivity coefficients.

These 1-D reactive transport results are shown primarily for illustrative purposes. Evaluation of the sensitivity of the reactive transport model results to the various flow, transport, and reaction parameters and boundary conditions (leak scenarios) was considered to be beyond the scope of this investigation. Data from only two physical sampling locations are insufficient for meaningful model calibration. However, based on the 1-D model results, two of the water leak scenarios were selected and used in 3-D flow and K_d-based transport modeling, as described in the following section.

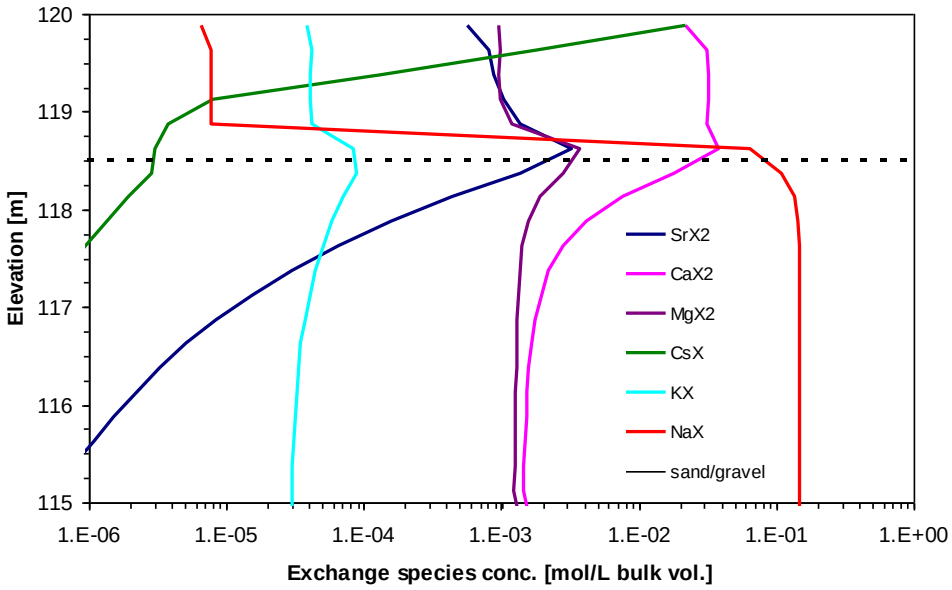

Figure 3.2. Simulated distributions of modeled exchangeable cations after 25 years (2011) for the 50 gal/wk water discharge rate.

3.3 Three-Dimensional Flow and Transport Modeling

A three-dimensional STOMP model was developed to estimate the spatial distribution of ^{90}Sr and ^{137}Cs in the subsurface beneath the 324 Building. The modeled domain is 37 m × 37 m × 15 m in the *x*-, *y*-, and *z*-directions, respectively. Figure 3.3 shows an oblique view of the modeled domain superimposed by a computer-assisted design (CAD) rendition of the B-Cell and Geoprobe track machine used for installation of access tubes. Nonuniform grid spacing was used in all coordinate directions, but uniform 0.5-m × 0.5-m spacing was used in the *x*–*y* directions for grid blocks used as source terms for water and contaminants (Figure 3.4). The vertical discretization of the grid blocks used for source terms is 0.1 m. As noted previously, the source grid blocks are aligned in a rectangular pattern that coincides approximately with the plan-view outline of the expansion joints in the concrete foundation of the B-Cell pad, through which the leak was presumed to have emanated.

Hydrostatic and outflow boundary conditions were specified for flow and transport, respectively, on all lateral boundaries. No-flow conditions were specified for both flow and transport on the upper boundary, with one exception that will be described later. Fixed aqueous pressure and outflow boundary conditions were specified for flow and transport, respectively, on the lower boundary; the water table was located at an elevation of 105 m. Water and contaminant associated with the B-Cell leak were introduced through source terms in some of the upper-most grid blocks, whose *x*–*y* locations correspond

approximately to the locations of the expansion joints at the bottom of the foundation underlying B-Cell, through which the spill is assumed to have seeped, based on the exposure rate measurements.

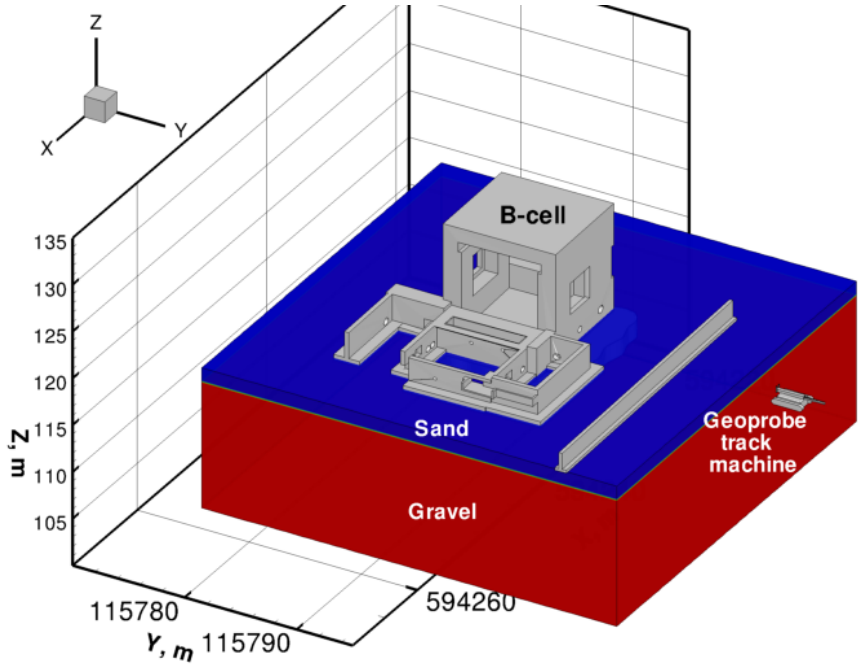

Figure 3.3. Oblique view of domain used for three-dimensional modeling, showing B-Cell, underlying sediments, and Geoprobe track machine used for installation of access tubes. The modeled domain is 37 m ×37 m × 15 m, in the *x*-, *y*-, and *z*-directions, respectively.

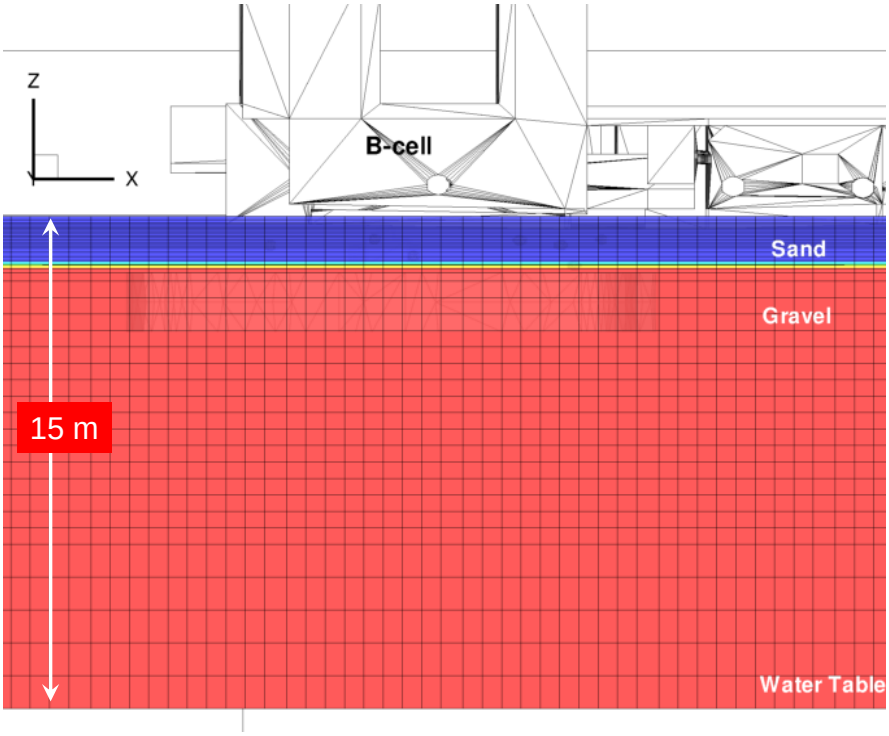

Figure 3.4. Spatial discretization of the three-dimensional model for a portion of the domain.

Initial attempts to run the 3-D flow and transport model, including the full reaction network used for the 1-D simulations, were unsuccessful due to excessive run times on available workstations. In principle, these calculations could be readily performed on a parallel version of STOMP, called eSTOMP. However, eSTOMP is currently considered to be a research code, and, as such, it has not been fully tested and qualified for this type of application. Also, insufficient resources were available in this limited investigation to perform the necessary testing of eSTOMP and to formally document the test results. Therefore, 3-D flow and transport simulations were performed using a serial version of STOMP that has been subjected to the required testing, documentation, and configuration management controls. Due to computational constraints, a linear adsorption isotherm (K_d) model was used for 3-D modeling instead of the full reaction network.

3.3.1 Selection of Partitioning Coefficients

Representing sorption processes using a linear isotherm model with a constant adsorption coefficient, or K_d value, is strictly valid only when chemical conditions are relatively constant and similar to those for which the K_d values were determined. In the case of the B-Cell spill, chemical conditions are likely to have varied significantly. However, in this case, as with many others, limited data, data and source term uncertainties, the larger computational effort of reactive transport simulations, and fiscal constraints dictated the use of the simpler K_d approach for 3-D flow and transport modeling.

Last et al. (2006) and Cantrell et al. (2007) have compiled data packages for Hanford waste site assessments. Both reports contain tables listing recommended K_d values and ranges for different waste chemistry/source categories. The reader is referred to Cantrell et al. (2007) for details on how the recommended K_d values and ranges were estimated. Table 3.7 shows a partial compilation of results from Cantrell et al. (2007) for strontium and cesium. Clearly, a wide range of K_d values and sorption behavior is possible for these two species, depending on chemical conditions and sediment characteristics. From the available data on the aqueous chemistry of the fluids leaked from B-Cell (Tables 3.1–3.3), it is difficult to choose a representative waste chemistry/source category from Table 3.7. Therefore, the use of mechanistic reactive transport models is desirable. However, the data requirements and computational demands for such models are significantly greater than simple sorption models.

Given the available information, K_d values from the lower end of the range shown in Table 3.7 were used for simulating two water release scenarios with a 3-D model. If the leaked waste solution was initially as acidic as is indicated by Table 3.1, then the effective K_d values could have initially been very low or even negligible (zero). As the acid waste was buffered by the concrete foundation of B-Cell and by the underlying sediments, the effective K_d values would have increased. The K_d values shown in Table 3.8 were used for model simulations. These K_d values are within the range of values listed in Table 3.7 but were selected so that the simulation results approximately matched the measured activities of ^{137}Cs and ^{90}Sr at the two sampled locations for the two modeled water release scenarios.

As noted previously, the gravel (actually muddy sandy gravel) contains a larger fraction of fine-grained particles than does the overlying sand. The measured CEC value for this material is also greater than that of the overlying sand. Therefore, larger K_d values were assigned to the gravel and smaller K_d values to the sand (Table 3.8). These K_d assignments are counterintuitive based solely on the names *sand* and *gravel*. However, these parameter assignments are more reflective of the differences in the actual textural characteristics and the measured CEC values for the two sediments.

Table 3.7. Estimated K_d values for strontium and cesium for different waste chemistry/source categories and impact factors (from Cantrell et al. 2007). See text for description of parameter assignments.

Analyte	High Impact			Intermediate Impact – Sand			Intermediate Impact – Gravel		
Waste Chemistry/Source Category 1: Very Acidic									
	K_d estimate [mL/g]			K_d estimate [mL/g]			K_d estimate [mL/g]		
	Best	Min	Max	Best	Min	Max	Best	Min	Max
Sr	10	5	15	22	10	50	6.8	3.1	15.5
Cs	1000	200	10000	2000	200	10000	620	62	3100
Waste Chemistry/Source Category 2: Very High Salt/Very Basic									
	K_d estimate [mL/g]			K_d estimate [mL/g]			K_d estimate [mL/g]		
	Best	Min	Max	Best	Min	Max	Best	Min	Max
Sr	22	10	50	22	10	50	6.8	3.1	15.5
Cs	10	0	500	100	10	1000	31	3.1	310
Waste Chemistry/Source Category 3: Chelate/High Salts									
	K_d estimate [mL/g]			K_d estimate [mL/g]			K_d estimate [mL/g]		
	Best	Min	Max	Best	Min	Max	Best	Min	Max
Sr	1	0.2	20	10	5	20	3.1	1.6	6.2
Cs	10	0	500	100	10	1000	31	3.1	310
Waste Chemistry/Source Category 4: Low Organic/Low Salt/Near Neutral									
	K_d estimate [mL/g]			K_d estimate [mL/g]			K_d estimate [mL/g]		
	Best	Min	Max	Best	Min	Max	Best	Min	Max
Sr	22	10	50	22	10	50	7	3	16
Cs	2000	200	10000	2000	200	10000	620	62	3100

Table 3.8. Sorption coefficients (K_d values) used for 3-D flow and transport modeling.

		K_d (cm^3/g)	
Water leak rate (gal/wk)	Species	Sand	Gravel (msG)
50	^{90}Sr	1.0	2.4
50	^{137}Cs	1.5	3.6
100	^{90}Sr	2.0	3.4
100	^{137}Cs	3.4	4.9

3.3.2 Three-Dimensional Simulation Results

None of the physical, hydraulic, or geochemical properties or water release rates and chemical composition of the leaked waste are known with certainty. However, with measurements of radionuclide activities at only two sampling locations beneath the B-Cell, calibrating the 3-D K_d-based model was a straightforward process. As shown in Figure 3.5, very similar transport results were obtained for two different water release rate scenarios with only small adjustments to the applied K_d values. The K_d values

required to obtain approximate matches to the measured activities for the two sample points are on the lower end of the range of values shown in Table 3.7.

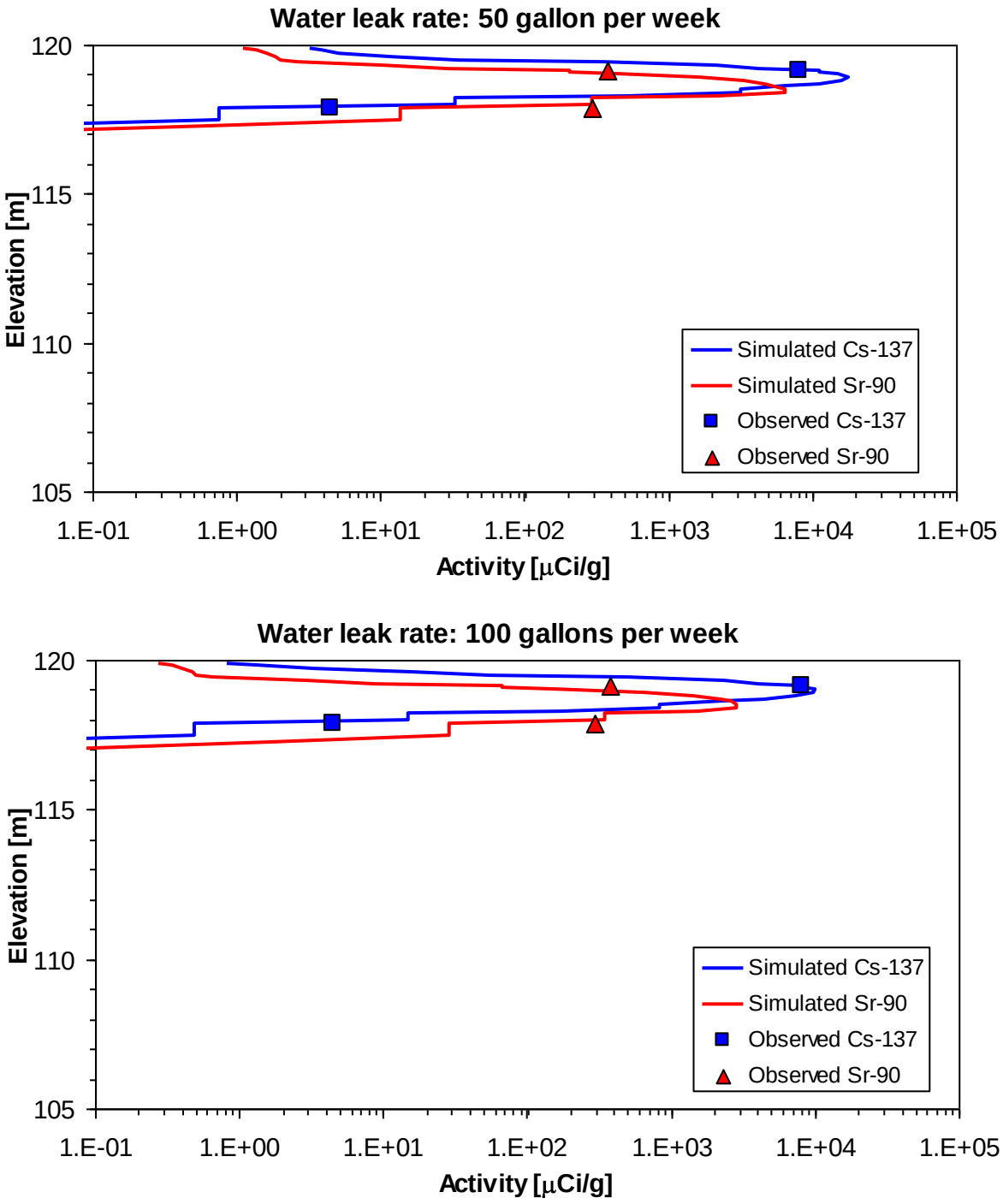

Figure 3.5. Vertical profiles of simulated ^{137}Cs and ^{90}Sr activities through the locations of the two physical sampling points for 50- and 100-gal/wk water leak rate scenarios, and the measured activities for the two sample points. The K_d values used for these simulations are listed in Table 3.8.

The 1-D and 3-D models yield differing results in terms of the predicted depths to peak concentrations and the maximum depths of penetration of the contaminants. This is an expected result because of differences in dimensionality and processes represented by the models. The 1-D reactive transport model results, which are assumed to be conservative, suggest that the highest concentrations of ^{137}Cs are located immediately below the foundation of the B-Cell, but that ^{137}Cs contamination may extend 3–7 m below the foundation, depending on the assumed water release rate. The 1-D reactive transport results suggest that peak concentrations of ^{90}Sr may be located 1–3 m below the foundation, but that ^{90}Sr contamination may extend 4–11 m below the foundation, again depending on the assumed water release rate. In contrast, the 3-D K_d-based model results suggest that for both ^{137}Cs and ^{90}Sr peak concentrations may be located 1–2 m below the foundation, and nearly all of the contamination may be contained within the upper 3 m of the sediment profile. The simulated peak ^{90}Sr concentrations for the 3-D K_d-based model are lower in magnitude and approximately 0.5 m deeper in the profile below the foundation of the B-Cell, relative to the simulated peak ^{137}Cs concentrations. Additional field data would be needed to better constrain model input specifications in order to reduce the uncertainty in model predictions.

The character of the K_d-based model results shown in Figure 3.5 differs significantly from that of the reactive transport model results shown in Figure 3.1 for several reasons. The K_d-based model is 3-D whereas the reactive transport model represents a 1-D vertically oriented column. Therefore, the 3-D model allows for lateral spreading of water and contaminants while the 1-D model does not. Sorption of ^{90}Sr and ^{137}Cs in the 1-D reactive transport model is based on an ion-exchange model that accounts for the finite sorption capacity of the sediments, as represented by measured values of CEC. Occupancy of exchange sites by different cations is a competitive process dictated by the aqueous composition of the pore water (or leaked waste) and experimentally based selectivity coefficients. The K_d-based sorption model used for 3-D modeling does not have a finite sorption capacity and does not consider the aqueous composition of the pore water. It is also important to note again that radioactive decay was not accounted for in the 1-D reactive transport modeling results, but it was accounted for in the 3-D K_d-based modeling results. The deeper penetration of ^{137}Cs and ^{90}Sr into the sediment profile and higher peak concentrations for the 1-D reactive transport case are results of these differences.

The 1-D reactive transport modeling results should be conservative in terms of predicted peak activities, as long as the total simulated activities of radionuclides released from the B-Cell are similar in magnitude to what was actually released. The 1-D reactive transport modeling results are probably also conservative in terms of predicted maximum depth of penetration of the contaminants, as long as the simulated water release rates were similar to what was actually applied. However, it should be emphasized that these results are based on very limited data and numerous assumptions. Additional sediment characterization and calibration data would be needed to determine whether or not geochemical reactions and possibly other processes (e.g., nonisothermal conditions, two-phase flow, changes in porosity and permeability due to precipitation-dissolution reactions) would be needed in the 3-D simulations to improve model fidelity.

Three-dimensional cutaway views of the total ^{137}Cs and ^{90}Sr concentration (grams per liter bulk volume) distributions and aqueous concentration (grams per liter aqueous phase) distribution for a conservative tracer from the 50-gal/wk water release rate scenario are shown in Figure 3.6. Three-dimensional views of the ^{137}Cs and ^{90}Sr and conservative tracer distributions for the 100-gal/wk water release rate scenario are shown in Figure 3.7.

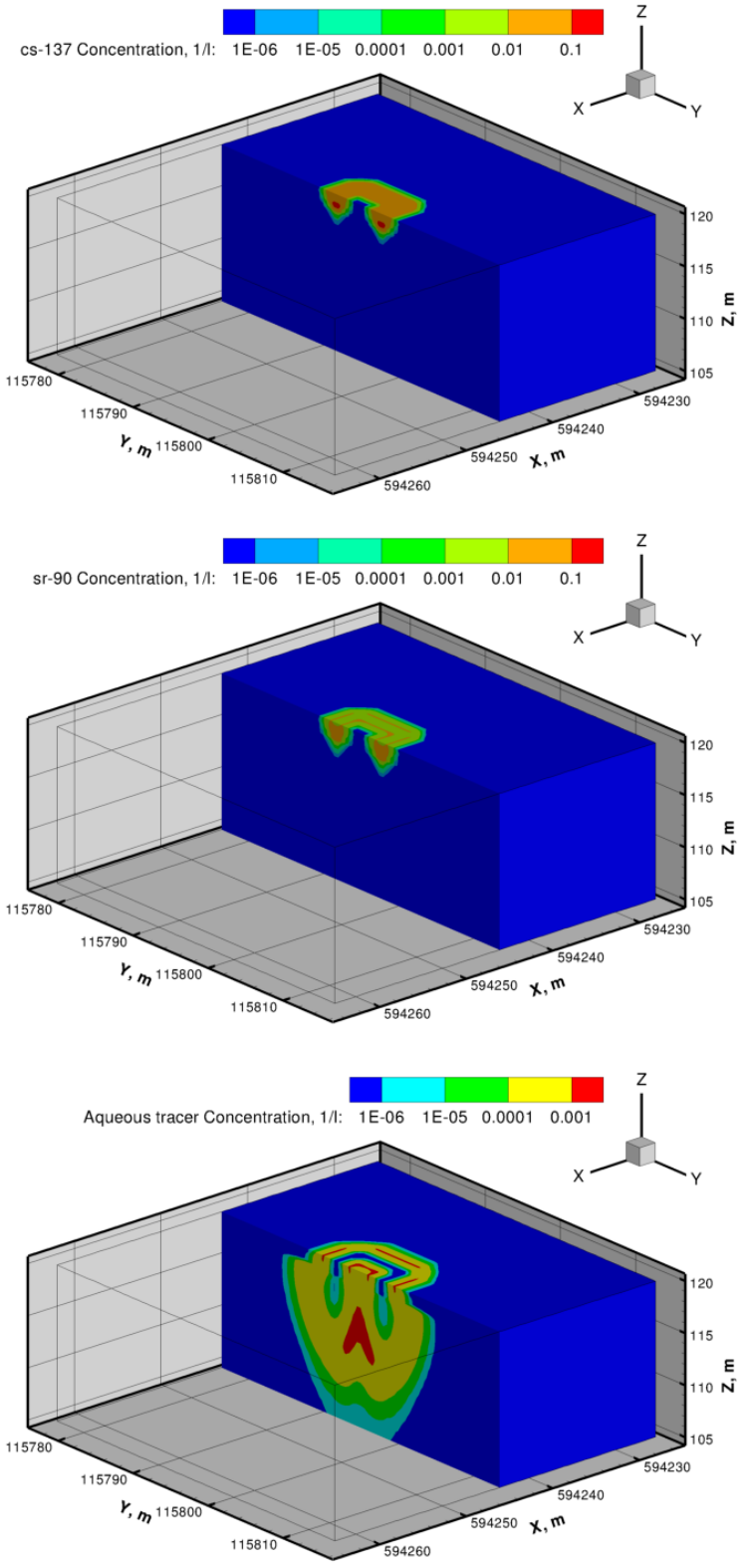

Figure 3.6. Simulated total ^{137}Cs and ^{90}Sr (grams per liter bulk volume) and aqueous tracer concentration (grams per liter aqueous phase) distributions for the 50-gal/wk water release rate scenario.

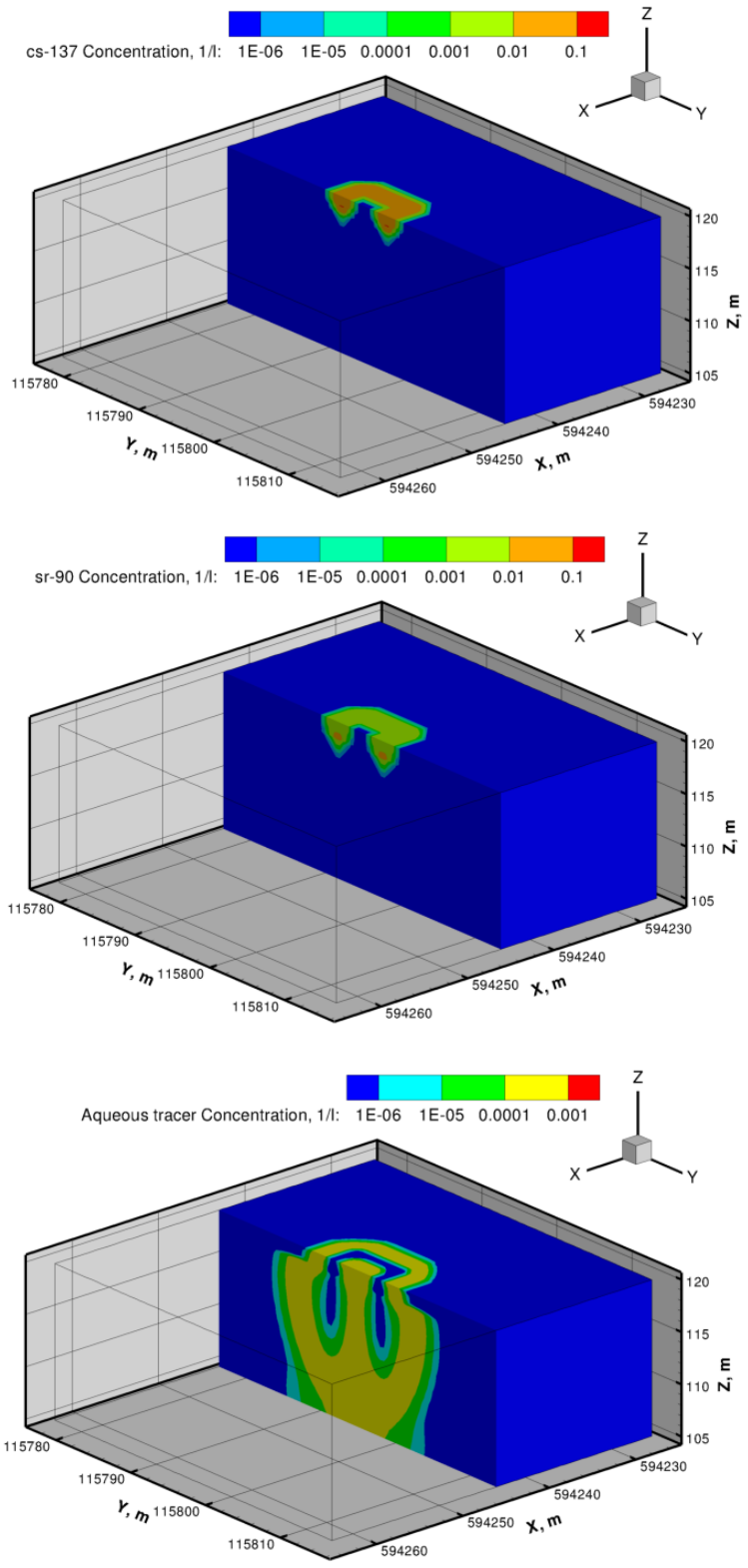

Figure 3.7. Simulated total ^{137}Cs and ^{90}Sr (grams per liter bulk volume) and aqueous tracer concentration (grams per liter aqueous phase) distributions for the 100-gal/wk water release rate scenario.

Vertical profiles of the observed and simulated water contents for the neutron probe measurement locations are shown for the 50- and 100-gal/wk water release rate scenarios in Figures 3.8 and 3.9, respectively. For both simulation cases, a 200-mm/yr flux of water was specified along the top northern boundary of the modeled domain starting in 2010 to represent infiltration into the exposed pit on the north side of the 324 Building. Without this added water, simulated water content profiles would not reproduce the observed pattern of the field-measured water contents near the top of the profile, which corresponds also to the northern end of the model domain where the access pipes entered the subsurface from the excavated pit.

The simulated water content profiles for these two cases at the measurement locations are nearly indistinguishable. This apparent insensitivity of simulated water contents at the measurement locations to water release rate is a result of the fact that the two simulated water release rates are both relatively small and 21 years has elapsed in the model simulations from the time when water additions were ceased (1991) to the time when water contents were monitored or measured (2011). Therefore, most of the added water has redistributed in the model simulations.

Figure 3.10 shows 3-D views of the predicted water content distributions for the two simulation cases after 26 years (in 2012). Although water additions from the simulated leak have mostly dissipated from under the B-Cell, evidence of this added water is still apparent. The impact of simulated water intrusion from the pit located on the north side of the domain is also clearly evident.

Differences between simulated and field-measured water contents can be attributed to several factors. The conceptual model used for simulations represents a simple two-layer system consisting of a thin sand layer overlying a thick gravel layer. The field-measured water content data suggest that this conceptual model is overly simplified and the actual sediment profile is much more heterogeneous. However, measurements of physical and hydraulic properties were available for only two bucket samples collected from the pit excavated on the north side of the 324 Building. Given the added uncertainties in water release rates from the B-Cell, the evolving natural groundwater recharge rates resulting from surface disturbance around the 324 Building, and possible impacts of waste chemistry on sediment properties, it would be difficult to reduce all the uncertainties to the extent that natural heterogeneity could be clearly distinguished from other factors. Additional characterization data would be needed to justify increasing the complexity of model structure.

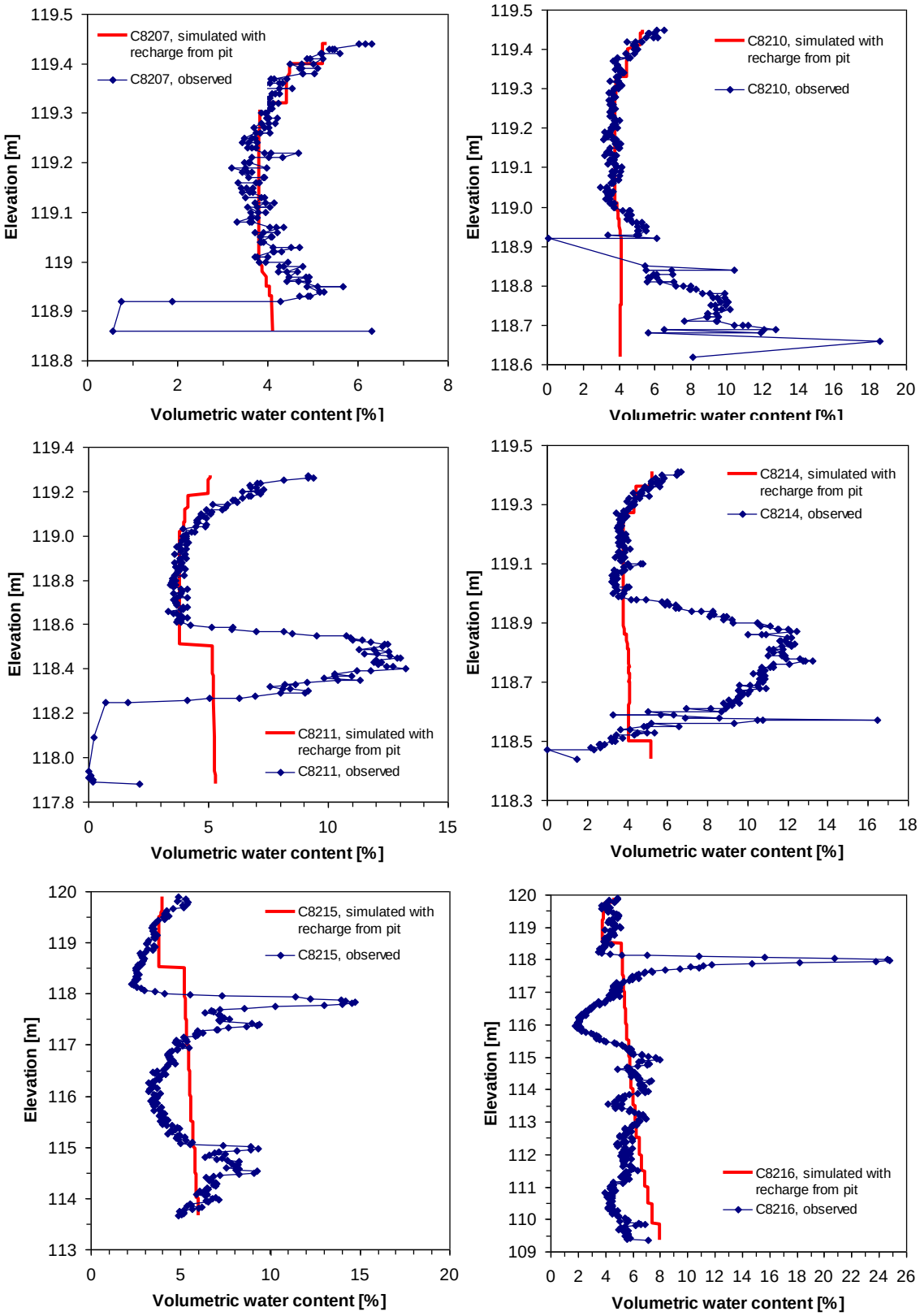

Figure 3.8. Observed and simulated water content profiles for the 50-gal/wk water release rate scenario at the neutron probe measurement locations.

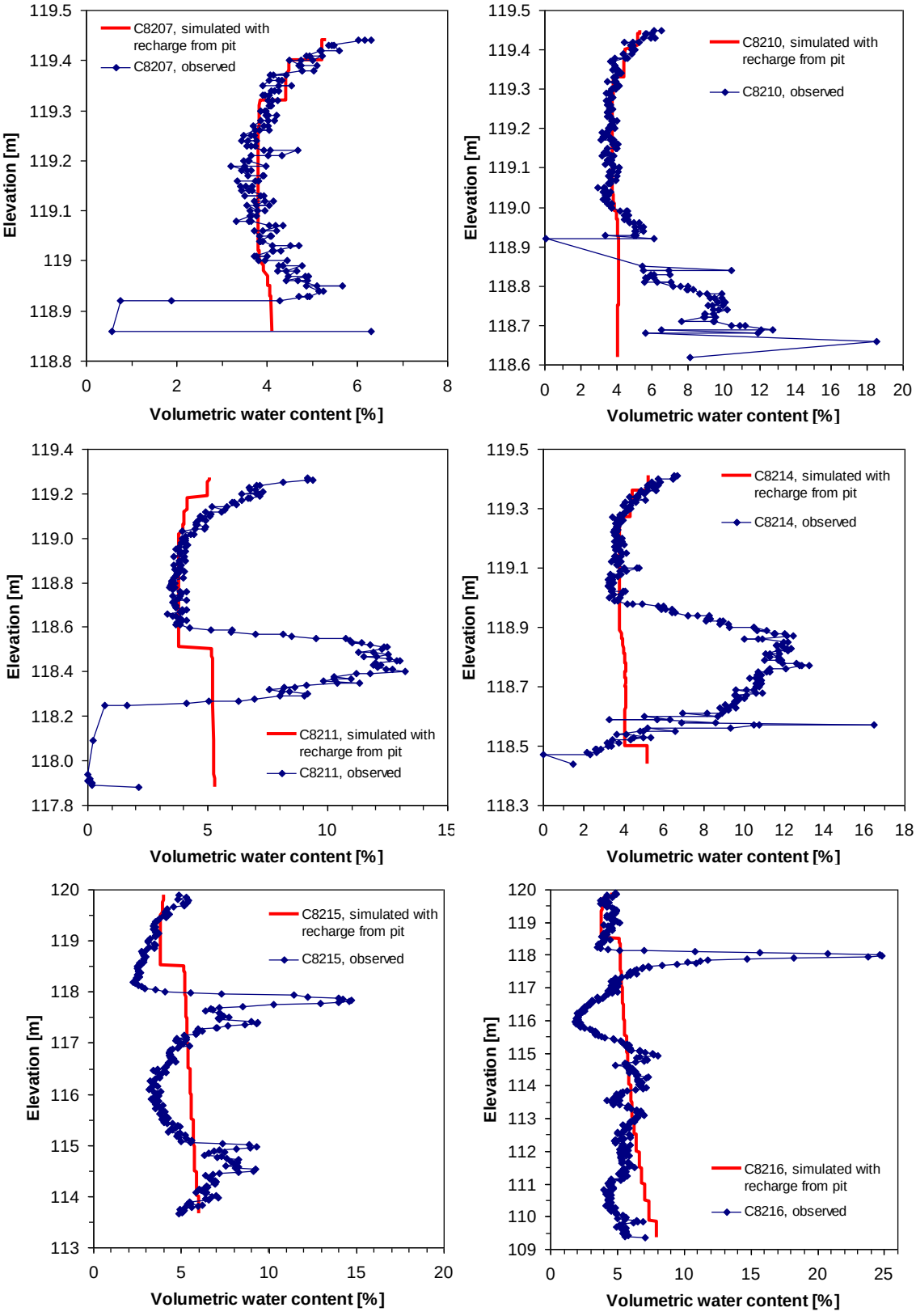

Figure 3.9. Observed and simulated water content profiles for the 100-gal/wk water release rate scenario at the neutron probe measurement locations.

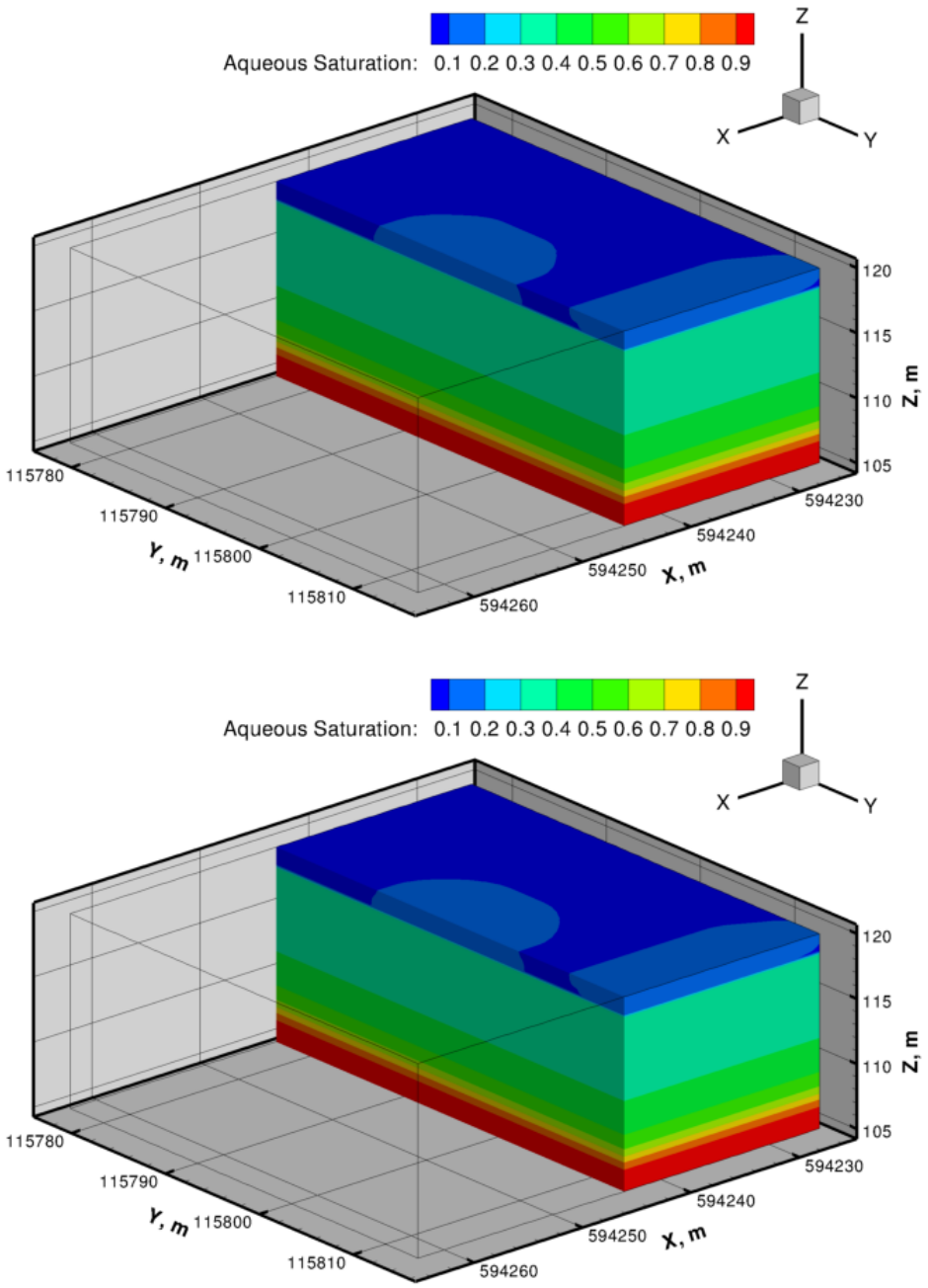

Figure 3.10. Cutaway views of aqueous saturation distributions for the 50-gal/wk (top) and 100-gal/wk (bottom) simulations cases, showing effects of added water from the B-Cell leak and from recharge on the top north side of the modeled domain.

4.0 Conclusions and Recommendations

One- and three-dimensional flow and transport modeling were performed to evaluate the possible extent of migration of ^{137}Cs and ^{90}Sr that leaked from the B-Cell into the subsurface underlying the 324 Building. The 1-D reactive transport and 3-D K_d-based models yielded differing results in terms of the predicted depths to peak concentrations and the maximum depths of penetration of the contaminants. The 1-D reactive transport model results, which are assumed to be conservative, suggest that the highest concentrations of ^{137}Cs are located immediately below the foundation of the B-Cell. However, the ^{137}Cs contamination may extend 3–7 m below the foundation, depending on the assumed water release rate. The 1-D reactive transport results suggest that peak concentrations of ^{90}Sr may be located 1–3 m below the foundation, but ^{90}Sr contamination may extent 4–11 m below the foundation, again depending on the assumed water release rate. In contrast, the 3-D Kd-based model results suggest that both ^{137}Cs and ^{90}Sr peak concentrations may be located 1–2 m below the foundation, and nearly all of the contamination may be contained within the upper 3 m of the sediment profile. The depth to the average position of the water table is approximately 15 m. The differences in results were not unexpected, owing to differences in dimensionality and processes represented in the models. Both models predict contaminant transport into the vadose zone but the contaminants not reaching the saturated zone.

The assumptions and parameter definitions underlying the flow and transport models were based on very limited site characterization data and are thus subject to significant, albeit unquantified, uncertainty.

Uncertainties in model inputs included

- initial volume and chemical composition of the spill
- volume and chemical composition of water used to wash the floor of B-Cell after the spill
- physical, chemical, hydraulic, and transport properties of concrete and subsurface materials underlying the 324 Building.

Additional field and laboratory characterization data would be needed to better constrain model input parameters in order to reduce the uncertainty in model predictions.

Based on the available data and simulation results, the remediation contractor (WCH) should plan for an excavation depth of at least 3 m below the base of the B-Cell foundation. However, given the paucity of data on water release rates, physical and hydraulic properties, and other key factors, and the associated uncertainties in modeling results, excavation beyond the 3-m depth could easily be required. Excavation will simply need to continue until measured concentrations or activities are low enough to be deemed acceptable.

Another possible alternative would be to cocoon the B-Cell, as has been done for several nuclear reactors along the Columbia River corridor, and to maintain it under institutional control until radioactivity has diminished to safe levels. Both ^{137}Cs and ^{90}Sr are relatively short-lived isotopes with half-lives of 30 and 29 years, respectively, so their original activities have already been diminished by nearly one-half. However, the original activities of the leaked fluids were quite high, so natural attenuation may not be a feasible remediation alternative.

Additional characterization could help to reduce some of the uncertainties associated with the distribution of contaminants in the subsurface underlying the 324 Building. If additional data were to be collected, several vertical boreholes should be installed around the periphery of the 324 Building, including one located downgradient (southeast) of the B-Cell. Neutron moisture and spectral gamma logging should be performed in these boreholes to determine the distributions of water content and the primary gamma-emitting radionuclides. In particular, ^{40}K and ^{232}Th have been shown to be strongly correlated with sediment textural characteristics. Physical and hydraulic properties should be determined on core samples from selected depth intervals. The downgradient borehole could be completed as a shallow groundwater monitoring well to augment the current 300 Area groundwater monitoring network because there currently are no groundwater monitoring wells near the 324 Building. It would also be helpful to have additional physical samples collected from slant boreholes that would target other areas under the B-Cell. Analysis of radionuclide activities at other locations for actual physical samples would provide the most definite information about contaminant distributions.

Finally, field-measured water content distributions and simulation results suggest that the pit excavated on the north side of the 324 Building to provide access to the subsurface is resulting in increased water contents under the building due to infiltration of natural precipitation. If the contaminated sediments underlying the B-Cell are excavated and removed relatively soon (1–2 years), then this increasing moisture will likely have little or no consequence. However, if the remediation effort is delayed, the increasing moisture could eventually result in mobilization of contaminants under the B-Cell and transport to groundwater.

5.0 References

40 CFR 141.66, "Federal Safe Drinking Water Act," *Code of Federal Regulations,* Subpart G – National Primary Water Regulations: Maximum Contaminant Levels and Maximum Residual Disinfectant Levels; Maximum Contaminant Levels for Radionuclides, as amended.

Appelo CAJ. 1994. Some calculations on multi-component transport with cation exchange in aquifers. *Ground Water* 32:968–975.

Babcock KL and RK Shulz. 1970. Isotopic and conventional determination of exchangeable sodium percentage of soil in relation to plant growth. *Soil Science* 109:19–22.

Bjornstad BN, JA Horner, VR Vermeul, DC Lanigan, and PD Thorne. 2009. *Borehole Completion and Conceptual Hydrogeologic Model for the IFRC Well Field, 300 Area, Hanford Site – Integrated Field Research Challenge Project*. PNNL-18340, Pacific Northwest National Laboratory, Richland, Washington.

Brooks RH and AT Corey. 1964. *Hydraulic Properties of Porous Media*. Hydrology Paper No. 3, Colorado State University, Fort Collins, Colorado.

Burdine NT. 1953. Relative permeability calculations from pore-size distribution data. *Transactions of the American Institute of Mining, Metallurgical and Petroleum Engineers* 198:71–78.

Cantrell KJ, JM Zachara, PE Dresel, KM Krupka, and RJ Serne. 2007. *Geochemical Processes Data Package for the Vadose Zone in the Single-Shell Tank Waste Management Areas at the Hanford Site*. PNNL-16663, Pacific Northwest National Laboratory, Richland, Washington.

Dane JH and JW Hopmans. 2002. Hanging water column. In JH Dane and GC Topp (eds), *Methods of Soil Analysis. Part 4: Physical Methods*, pp. 680-683. SSSA Book Series 5, Science Society of America, Madison, Wisconsin.

Folk RL. 1980. *Petrology of Sedimentary Rocks*. Hemphill Publishing Company, Austin, Texas.

Gaines GL and HC Thomas. 1953. Adsorption studies on clay minerals, II. A formulation of the thermodynamics of exchange adsorption. *Journal of Chemical Physics* 21:714–718.

Gee GW and D Or. 2002. Particle-size analysis. In JH Dane and GC Topp (eds), *Methods of Soil Analysis. Part 4: Physical Methods*, pp. 255–293. SSSA Book Series 5, Science Society of America, Madison, Wisconsin.

Hartman MJ, LF Morasch, and WD Webber (eds). 2007. *Hanford Site Groundwater Monitoring for Fiscal Year 2006.* PNNL-16346, Pacific Northwest National Laboratory, Richland, Washington.

LANL. 2005. *MCNP – A General Monte Carlo N-Particle Transport Code, Version 5*. LA-UR-03-1987, Los Alamos National Laboratory, Los Alamos, New Mexico.

Last GV, EJ Freeman, KJ Cantrell, MJ Fayer, GW Gee, WE Nichols, BN Bjornstad, and DG Horton. 2006. *Vadose Zone Hydrogeology Data Package for Hanford Assessments*. PNNL-14702, Rev. 1, Pacific Northwest National Laboratory, Richland, Washington.

Lichtner P and JM Zachara. 2005. *Modeling Batch Reactor Ion Exchange Experiments of Strontium-Calcium-Magnesium-Potassium-Sodium on Hanford Sediments*. RPP-10098, Rev. 0, Appendix D, CH2M-Hill Hanford, Richland, Washington.

Liu C, JM Zachara, and SC Smith. 2004. A cation exchange model to describe Cs+ sorption at high ionic strength in subsurface sediments at Hanford site, USA. *Journal of Contaminant Hydrology* 68:217–238.

Ma R, C Zheng, H Prommer, J Greskowiak, C Liu, J Zachara, and M Rockhold. 2010. A field-scale reactive transport model for U(VI) migration influenced by coupled multirate mass transfer and surface complexation reactions. *Water Resources Research* 46:W05509. doi:10.1029/2009WR008168.

McKinley J, J Zachara, S Smith, and C Liu. 2007. Cation exchange reactions controlling desorption of $^{90}Sr^{2+}$ from coarse-grained contaminated sediments at the Hanford site, Washington. *Geochimica et Cosmochimica Acta* 71(2):305–325.

Mualem Y. 1976. A new model for predicting the hydraulic conductivity of unsaturated porous media. *Water Resources Research* 12(3):513–522.

ORNL. 1980. *A User's Manual for the ORIGEN2 Computer Code*. ORNL/TM-7175, Oak Ridge National Laboratory, Oak Ridge, Tennessee.

Palandri JL and YK Kharaka. 2004. *A Compilation of Rate Parameters of Water–Mineral Interaction Kinetics for Application to Geochemical Modeling*. Open File Report 2004-1068, U.S. Geological Survey, Menlo Park, California.

Papelis C and W Um. 2003. *Evaluation of Cesium, Strontium, and Lead Sorption, Desorption, and Diffusion in Volcanic Tuffs from Frenchman Flat, Nevada Test Site: Macroscopic and Spectroscopic Investigations*. DOE/NV/13609-18, Nevada Site Office, National Nuclear Security Administration, U.S. Department of Energy, Las Vegas, Nevada.

Poinssot C, B Baeyens, and MH Bradbury. 1999. Experimental and modelling studies of cesium sorption on illite. *Geochimica et Cosmochimica Acta* 63(19–20):3217–3227.

Reynolds WD, EG Youngs, A Amoozegar, HWG Booltink, and J Bouma. 2002. Saturated and field-saturated water flow parameters. In JH Dane and GC Topp (eds), *Methods of Soil Analysis. Part 4: Physical Methods*, pp. 797–817. SSSA Book Series 5, Science Society of America, Madison, Wisconsin.

Shaw. 2011. *Certificate of Analysis.* Project No. 135594.00210000, Report No. LION0311070, March 11, 2011, Shaw Environmental, Inc., Exton, Pennsylvania.

Sposito G. 1994. *Chemical Equilibrium and Kinetics in Soils*. Oxford University Press, New York.

Stumm W and JJ Morgan. 1996. *Aquatic Chemistry – Chemical Equilibria and Rates in Natural Waters*. 3rd edition. John Wiley & Sons, Inc., New York.

Valenta MM. 2008. *Cation Exchange Capacity Extractions*. AGG-CEC-001 Rev. 0, PNNL Technical Procedure, Pacific Northwest National Laboratory, Richland, Washington.

Valocchi AJ, RL Street, and PV Roberts. 1981. Transport of ion-exchanging solutes in groundwater: Chromatographic theory and field simulation. *Water Resources Research* 17:1517–1527.

van Genuchten M Th. 1980. A closed-form equation for predicting the unsaturated hydraulic conductivity of unsaturated soils. *Soil Science Society of American Journal* 44:892–898.

White MD and BP McGrail. 2005. *STOMP – Subsurface Transport Over Multiple Phases, Version 1.0 Addendum: ECKEChem Equilibrium-Conservation-Kinetic Equation Chemistry and Reactive Transport*. PNNL-15482, Pacific Northwest National Laboratory, Richland, Washington.

White MD and M Oostrom. 2006. *STOMP – Subsurface Transport Over Multiple Phases, Version 4.0 User's Guide*. PNNL-15782, Pacific Northwest National Laboratory, Richland, Washington.

Wolery TW and RL Jarek. 2003. *Software User's Manual, EQ3/6, Version 8.0*. Sandia National Laboratories, Albuquerque, New Mexico.

Zachara JM, SC Smith, C Liu, JP McKinley, RJ Serne, and PL Gassman. 2002. Sorption of Cs+ to micaceous subsurface sediments from the Hanford site, USA. *Geochimica et Cosmochimica Acta* 66(2):193–211.

Appendix

Analytical Data Report for Sediment Samples Collected from the 324 Building

01/24/12 17:26

To: Mark Rockhold

From: Michael J. Lindberg

Environmental Sciences Laboratory
Energy and Environment Directorate, Pacific Northwest National Laboratory

Subject: Analytical Data Report for Sediment Samples Collected For WCH Bldg. 324 , Sample Delivery Group ESL090022, SAF Number RC-147

This letter contains the following information for sample delivery group ESL090022

- Cover Sheet
- Narrative
- Analytical Results
- Quality Control

Introduction

On March 2, 2011, sediment samples were received from the 300 Area for geochemical studies.

Analytical Results/Methodology

The analyses for this project were performed at the 331 Building located in the 300 Area of the Hanford Site. The analyses were performed according to Pacific Northwest National Laboratory (PNNL) approved procedures and/or nationally recognized test procedures. The data sets include the sample identification numbers, analytical results, estimated quantification limits (EQL), and quality control data.

Quality Control

The preparatory and analytical quality control requirements, calibration requirements, acceptance criteria, and failure actions are defined in the on-line QA plan "Conducting Analytical Work in Support of Regulatory Programs" (CAW). This QA plan implements the Hanford Analytical Services Quality Assurance Requirements Documents (HASQARD) for PNNL.

Definitions

Dup	Duplicate
RPD	Relative Percent Difference
NR	No Recovery (percent recovery less than zero)
ND	Non-Detectable
%REC	Percent Recovery

Sample Receipt

Samples were received with a chain of custody (COC) and were analyzed according to the sample identification numbers supplied by the client. All Samples were refrigerated upon receipt until prepared for analysis.

All samples were received with custody seals intact unless noted in the Case Narrative.

Holding Times

Holding time is defined as the time from sample preparation to the time of analyses. The prescribed holding times were met for all analytes unless noted in the Case Narrative.

Analytical Results

All reported analytical results meet the requirements of the CAW or client-specified SOW unless noted in the case narrative.

Case Narrative Report

Hold Time:

Not Applicable

Preparation Blank (PB):

No discrepancies noted.

Duplicate (DUP):

No discrepancies noted.

Laboratory Control Samples (LCS):

Not applicable.

Post Spike (PS):

Post-Spike Recovery for Barium (70.1%) was outside acceptance limits (75-125) in 1C16004-PS1 for ICP-OES Vadose-CEC
Potential Matrix interference.

Post-Spike Recovery for Calcium (NR) was outside acceptance limits (75-125) in 1C16004-PS1 for ICP-OES Vadose-CEC
The native sample concentration of the sample was greater than 5 times the spike concentration. There should be not impact to data as reported.

Post-Spike Recovery for Magnesium (NR) was outside acceptance limits (75-125) in 1C16004-PS1 for ICP-OES Vadose-CEC
The native sample concentration of the sample was greater than 5 times the spike concentration. There should be not impact to data as reported.

Post-Spike Recovery for Sodium (49%) was outside acceptance limits (75-125) in 1C16004-PS1 for ICP-OES Vadose-CEC
Potential Matrix interference.

Matrix Spike (MS):

Not Applicable.

Other QC Criteria:

None noted.

I certify that this data package is in compliance with the SOW, both technically and for completeness, for other than the conditions detailed above. Release of the data contained in this hard copy data package has been authorized by the Laboratory Analytical Manager as verified by this signature.

Michael Lindberg

PACIFIC NORTHWEST NATIONAL LABORATORY
operated by
BATTELLE
for the
UNITED STATES DEPARTMENT OF ENERGY
under Contract DE-AC05-76RLOJ830

SAMPLES INCLUDED IN THIS REPORT

WCH 324 Soils

HEIS No.	Laboratory ID	Matrix	Date Collected	Date Received
J1DWN9-A	1103002-01	SOIL	1/27/11 09:15	3/2/11 09:44
J1DWP0-A	1103002-02	SOIL	1/27/11 09:40	3/2/11 09:44
J1DWN9-B	1103002-03	SOIL	1/27/11 09:15	3/2/11 09:44
J1DWP0-B	1103002-04	SOIL	1/27/11 09:40	3/2/11 09:44

The following analyses were performed on the following samples included in this report:

Alkalinity, Titrimetic (pH 4.5)

Cation Exchange Capacity

Metals CEC by ICPOES

Moisture Content

Particle Density of soil samples

Particle Size Distribution (Dry Sieve)

pH of Waters By Electrode

SAMPLES ANALYZED IN THIS REPORT

HEIS No.	Laboratory ID	Matrix	Date Collected	Date Received
J1DWN9-A	1103002-01	SOIL	1/27/11 09:15	3/2/11 09:44
J1DWP0-A	1103002-02	SOIL	1/27/11 09:40	3/2/11 09:44
J1DWN9-B	1103002-03	SOIL	1/27/11 09:15	3/2/11 09:44
J1DWP0-B	1103002-04	SOIL	1/27/11 09:40	3/2/11 09:44

Wet Chemistry

Alkalinity as CaCO3 (ug/g dry) by Standard Methods 2320B

Lab ID	HEIS No.	Results	EQL	Analyzed	Batch
1103002-01	J1DWN9-A	6.98E1	2.35E1	3/24/11	1C28001
1103002-02	J1DWP0-A	6.92E1	2.35E1	3/24/11	1C28001
1103002-03	J1DWN9-B	7.18E1	2.35E1	3/24/11	1C28001
1103002-04	J1DWP0-B	6.64E1	2.36E1	3/24/11	1C28001

Wet Chemistry

Moisture Content (% by Weight) by AGG-WC-001

Lab ID	HEIS No.	Results	EQL	Analyzed	Batch
1103002-01	J1DWN9-A	4.34E0	N/A	3/10/11	1C10001
1103002-02	J1DWP0-A	6.78E0	N/A	3/10/11	1C10001
1103002-03	J1DWN9-B	4.37E0	N/A	3/10/11	1C10001
1103002-04	J1DWP0-B	5.60E0	N/A	3/10/11	1C10001

Wet Chemistry

pH (pH Units) by AGG-pH-001

Lab ID	HEIS No.	Results	EQL	Analyzed	Batch
1103002-01	J1DWN9-A	8.82E0	N/A	3/22/11	1C22004
1103002-02	J1DWP0-A	8.61E0	N/A	3/22/11	1C22004
1103002-03	J1DWN9-B	8.81E0	N/A	3/22/11	1C22004
1103002-04	J1DWP0-B	8.56E0	N/A	3/22/11	1C22004

Total Metals by PNNL-AGG-ICP-AES

CAS #	Analyte	Results	Units	EQL	Analyzed	Batch	Method
HEIS No.	**J1DWN9-A**		**Lab ID:**	**1103002-01**			
7440-39-3	Barium	1.17E-2	mg/g dry	1.32E-4	3/16/11	1C16004	PNNL-AGG-ICP-AES
7440-70-2	Calcium	2.06E0	mg/g dry	1.78E-3	3/16/11	1C16004	PNNL-AGG-ICP-AES
7440-09-7	Potassium	9.26E-2	mg/g dry	1.07E-2	3/16/11	1C16004	PNNL-AGG-ICP-AES
7439-95-4	Magnesium	1.08E-1	mg/g dry	1.24E-4	3/16/11	1C16004	PNNL-AGG-ICP-AES
7440-24-6	Strontium	5.30E-3	mg/g dry	5.18E-4	3/16/11	1C16004	PNNL-AGG-ICP-AES
7440-23-5	Sodium	5.88E-3	mg/g dry	1.62E-3	3/16/11	1C16004	PNNL-AGG-ICP-AES
HEIS No.	**J1DWP0-A**		**Lab ID:**	**1103002-02**			
7440-39-3	Barium	1.41E-2	mg/g dry	1.35E-4	3/16/11	1C16004	PNNL-AGG-ICP-AES
7440-70-2	Calcium	2.24E0	mg/g dry	1.82E-3	3/16/11	1C16004	PNNL-AGG-ICP-AES
7440-09-7	Potassium	9.25E-2	mg/g dry	1.10E-2	3/16/11	1C16004	PNNL-AGG-ICP-AES
7439-95-4	Magnesium	3.29E-1	mg/g dry	1.27E-4	3/16/11	1C16004	PNNL-AGG-ICP-AES
7440-24-6	Strontium	9.28E-3	mg/g dry	5.30E-4	3/16/11	1C16004	PNNL-AGG-ICP-AES
7440-23-5	Sodium	1.64E-2	mg/g dry	1.66E-3	3/16/11	1C16004	PNNL-AGG-ICP-AES
HEIS No.	**J1DWN9-B**		**Lab ID:**	**1103002-03**			
7440-39-3	Barium	1.15E-2	mg/g dry	1.32E-4	3/16/11	1C16004	PNNL-AGG-ICP-AES
7440-70-2	Calcium	2.05E0	mg/g dry	1.79E-3	3/16/11	1C16004	PNNL-AGG-ICP-AES
7440-09-7	Potassium	9.05E-2	mg/g dry	1.08E-2	3/16/11	1C16004	PNNL-AGG-ICP-AES
7439-95-4	Magnesium	1.01E-1	mg/g dry	1.25E-4	3/16/11	1C16004	PNNL-AGG-ICP-AES
7440-24-6	Strontium	5.19E-3	mg/g dry	5.20E-4	3/16/11	1C16004	PNNL-AGG-ICP-AES
7440-23-5	Sodium	6.10E-3	mg/g dry	1.63E-3	3/16/11	1C16004	PNNL-AGG-ICP-AES
HEIS No.	**J1DWP0-B**		**Lab ID:**	**1103002-04**			
7440-39-3	Barium	1.42E-2	mg/g dry	1.34E-4	3/16/11	1C16004	PNNL-AGG-ICP-AES
7440-70-2	Calcium	2.34E0	mg/g dry	1.81E-3	3/16/11	1C16004	PNNL-AGG-ICP-AES
7440-09-7	Potassium	9.64E-2	mg/g dry	1.09E-2	3/16/11	1C16004	PNNL-AGG-ICP-AES
7439-95-4	Magnesium	3.43E-1	mg/g dry	1.27E-4	3/16/11	1C16004	PNNL-AGG-ICP-AES
7440-24-6	Strontium	9.85E-3	mg/g dry	5.26E-4	3/16/11	1C16004	PNNL-AGG-ICP-AES
7440-23-5	Sodium	1.63E-2	mg/g dry	1.65E-3	3/16/11	1C16004	PNNL-AGG-ICP-AES

Physical Characteristics

Cation-exchange capacity of soils (meq/100 g) by CEC Ammonium Acetate

Lab ID	HEIS No.	Results	EQL	Analyzed	Batch
1103002-01	J1DWN9-A	1.15E1	N/A	1/24/12	2A24013
1103002-02	J1DWP0-A	1.42E1	N/A	1/24/12	2A24013
1103002-03	J1DWN9-B	1.13E1	N/A	1/24/12	2A24013
1103002-04	J1DWP0-B	1.49E1	N/A	1/24/12	2A24013

Particle Size Distribution (Dry Sieve)

CAS #	Analyte	Results	Units	EQL	Analyzed	Batch	Method
HEIS No.	**J1DWN9-A**		**Lab ID:**	**1103002-01**			
RETPAN	Particle Size Pan	2.82E-1	% Passing	N/A	3/10/11	0I23005	ASTM D422-63
PAS2.5IN	Particle Size 63000 uM	0	% Passing	N/A	3/10/11	0I23005	ASTM D422-63
PAS1.25IN	Particle Size 31500 uM	0	% Passing	N/A	3/10/11	0I23005	ASTM D422-63
PAS5/8IN	Particle Size 16000 uM	0	% Passing	N/A	3/10/11	0I23005	ASTM D422-63
PAS5/16IN	Particle Size 8000 uM	0	% Passing	N/A	3/10/11	0I23005	ASTM D422-63
PAS#5	Particle Size 4000 uM	0	% Passing	N/A	3/10/11	0I23005	ASTM D422-63
PAS#10	Particle Size 2000 uM	1.52E-2	% Passing	N/A	3/10/11	0I23005	ASTM D422-63
PAS#18	Particle Size 1000 uM	6.41E-1	% Passing	N/A	3/10/11	0I23005	ASTM D422-63
PAS#35	Particle Size 500 uM	2.93E1	% Passing	N/A	3/10/11	0I23005	ASTM D422-63
PAS#60	Particle Size 250 uM	5.23E1	% Passing	N/A	3/10/11	0I23005	ASTM D422-63
PAS#120	Particle Size 125 uM	1.49E1	% Passing	N/A	3/10/11	0I23005	ASTM D422-63
PAS#230	Particle Size 63 uM	2.66E0	% Passing	N/A	3/10/11	0I23005	ASTM D422-63
HEIS No.	**J1DWP0-A**		**Lab ID:**	**1103002-02**			
RETPAN	Particle Size Pan	2.20E0	% Passing	N/A	3/10/11	0I23005	ASTM D422-63
PAS2.5IN	Particle Size 63000 uM	0	% Passing	N/A	3/10/11	0I23005	ASTM D422-63
PAS1.25IN	Particle Size 31500 uM	1.37E1	% Passing	N/A	3/10/11	0I23005	ASTM D422-63
PAS5/8IN	Particle Size 16000 uM	2.38E1	% Passing	N/A	3/10/11	0I23005	ASTM D422-63
PAS5/16IN	Particle Size 8000 uM	1.63E1	% Passing	N/A	3/10/11	0I23005	ASTM D422-63
PAS#5	Particle Size 4000 uM	6.63E0	% Passing	N/A	3/10/11	0I23005	ASTM D422-63
PAS#10	Particle Size 2000 uM	4.12E0	% Passing	N/A	3/10/11	0I23005	ASTM D422-63
PAS#18	Particle Size 1000 uM	2.48E0	% Passing	N/A	3/10/11	0I23005	ASTM D422-63
PAS#35	Particle Size 500 uM	5.98E0	% Passing	N/A	3/10/11	0I23005	ASTM D422-63
PAS#60	Particle Size 250 uM	1.44E1	% Passing	N/A	3/10/11	0I23005	ASTM D422-63
PAS#120	Particle Size 125 uM	6.85E0	% Passing	N/A	3/10/11	0I23005	ASTM D422-63
PAS#230	Particle Size 63 uM	3.48E0	% Passing	N/A	3/10/11	0I23005	ASTM D422-63
HEIS No.	**J1DWN9-B**		**Lab ID:**	**1103002-03**			
RETPAN	Particle Size Pan	3.14E-1	% Passing	N/A	3/10/11	0I23005	ASTM D422-63
PAS2.5IN	Particle Size 63000 uM	0	% Passing	N/A	3/10/11	0I23005	ASTM D422-63
PAS1.25IN	Particle Size 31500 uM	0	% Passing	N/A	3/10/11	0I23005	ASTM D422-63
PAS5/8IN	Particle Size 16000 uM	0	% Passing	N/A	3/10/11	0I23005	ASTM D422-63
PAS5/16IN	Particle Size 8000 uM	0	% Passing	N/A	3/10/11	0I23005	ASTM D422-63
PAS#5	Particle Size 4000 uM	0	% Passing	N/A	3/10/11	0I23005	ASTM D422-63
PAS#10	Particle Size 2000 uM	1.01E-2	% Passing	N/A	3/10/11	0I23005	ASTM D422-63
PAS#18	Particle Size 1000 uM	6.54E-1	% Passing	N/A	3/10/11	0I23005	ASTM D422-63
PAS#35	Particle Size 500 uM	3.05E1	% Passing	N/A	3/10/11	0I23005	ASTM D422-63
PAS#60	Particle Size 250 uM	5.08E1	% Passing	N/A	3/10/11	0I23005	ASTM D422-63
PAS#120	Particle Size 125 uM	1.49E1	% Passing	N/A	3/10/11	0I23005	ASTM D422-63
PAS#230	Particle Size 63 uM	2.75E0	% Passing	N/A	3/10/11	0I23005	ASTM D422-63
HEIS No.	**J1DWP0-B**		**Lab ID:**	**1103002-04**			
RETPAN	Particle Size Pan	2.65E0	% Passing	N/A	3/10/11	0I23005	ASTM D422-63
PAS2.5IN	Particle Size 63000 uM	0	% Passing	N/A	3/10/11	0I23005	ASTM D422-63
PAS1.25IN	Particle Size 31500 uM	2.21E1	% Passing	N/A	3/10/11	0I23005	ASTM D422-63
PAS5/8IN	Particle Size 16000 uM	2.44E1	% Passing	N/A	3/10/11	0I23005	ASTM D422-63
PAS5/16IN	Particle Size 8000 uM	1.16E1	% Passing	N/A	3/10/11	0I23005	ASTM D422-63
PAS#5	Particle Size 4000 uM	5.44E0	% Passing	N/A	3/10/11	0I23005	ASTM D422-63
PAS#10	Particle Size 2000 uM	3.34E0	% Passing	N/A	3/10/11	0I23005	ASTM D422-63
PAS#18	Particle Size 1000 uM	2.09E0	% Passing	N/A	3/10/11	0I23005	ASTM D422-63
PAS#35	Particle Size 500 uM	5.59E0	% Passing	N/A	3/10/11	0I23005	ASTM D422-63

Particle Size Distribution (Dry Sieve)

CAS #	Analyte	Results	Units	EQL	Analyzed	Batch	Method
HEIS No.	**J1DWP0-B**		**Lab ID:**	**1103002-04**			
PAS#60	Particle Size 250 uM	1.20E1	% Passing	N/A	3/10/11	0I23005	ASTM D422-63
PAS#120	Particle Size 125 uM	6.76E0	% Passing	N/A	3/10/11	0I23005	ASTM D422-63
PAS#230	Particle Size 63 uM	4.03E0	% Passing	N/A	3/10/11	0I23005	ASTM D422-63

Particle Density

Particle Density (g/cc) by ASTM D854

Lab ID	HEIS No.	Results	EQL	Analyzed	Batch
1103002-01	J1DWN9-A	2.65E0	N/A	3/10/11	1C08016
1103002-02	J1DWP0-A	2.64E0	N/A	3/10/11	1C08016
1103002-03	J1DWN9-B	2.61E0	N/A	3/10/11	1C08016
1103002-04	J1DWP0-B	2.61E0	N/A	3/10/11	1C08016

Wet Chemistry - Quality Control
Environmental Science Laboratory

Analyte	Result	Reporting Limit	Units	Spike Level	Source Result	%REC	%REC Limits	RPD	RPD Limit	Notes
Batch 1C22004 - 1:1 Water Extract (pH_EC_Alk)										
Duplicate (1C22004-DUP1)		**Source: 1103002-04**		Prepared & Analyzed: 03/22/11						
pH	8.53E0	N/A	pH Units		8.56E0			0.351	35	
Batch 1C28001 - 1:1 Water Extract (pH_EC_Alk)										
Blank (1C28001-BLK1)				Prepared & Analyzed: 03/24/11						
Alkalinity as CaCO3	<2.35E1	2.35E1	ug/g wet							
Duplicate (1C28001-DUP1)		**Source: 1103002-04**		Prepared & Analyzed: 03/24/11						
Alkalinity as CaCO3	6.78E1	2.35E1	ug/g dry		6.64E1			2.16	35	

Total Metals by PNNL-AGG-ICP-AES - Quality Control

Environmental Science Laboratory

Analyte	Result	Reporting Limit	Units	Spike Level	Source Result	%REC	%REC Limits	RPD	RPD Limit	Notes
Batch 1C16004 - CEC Extract (ICP/ICPMS)										
Blank (1C16004-BLK1)				Prepared & Analyzed: 03/16/11						
Barium	<3.63E-5	3.63E-5	mg/g wet							
Calcium	<4.90E-4	4.90E-4	"							
Potassium	<2.96E-3	2.96E-3	"							
Magnesium	<3.43E-5	3.43E-5	"							
Strontium	<1.43E-4	1.43E-4	"							
Sodium	<4.47E-4	4.47E-4	"							
Blank (1C16004-BLK2)				Prepared & Analyzed: 03/16/11						
Barium	<3.63E-5	3.63E-5	mg/g wet							
Calcium	<4.90E-4	4.90E-4	"							
Potassium	<2.96E-3	2.96E-3	"							
Magnesium	<3.43E-5	3.43E-5	"							
Strontium	<1.43E-4	1.43E-4	"							
Sodium	<4.47E-4	4.47E-4	"							
Duplicate (1C16004-DUP1)	**Source: 1103002-02**			Prepared & Analyzed: 03/16/11						
Barium	1.49E-2	1.35E-4	mg/g dry		1.41E-2			5.55	20	
Calcium	2.37E0	1.82E-3	"		2.24E0			5.71	20	
Potassium	9.70E-2	1.10E-2	"		9.25E-2			4.78	20	
Magnesium	3.31E-1	1.28E-4	"		3.29E-1			0.746	20	
Strontium	9.86E-3	5.31E-4	"		9.28E-3			6.04	20	
Sodium	1.70E-2	1.66E-3	"		1.64E-2			4.11	20	
Duplicate (1C16004-DUP2)	**Source: 1103002-01**			Prepared & Analyzed: 03/16/11						
Barium	1.09E-2	1.32E-4	mg/g dry		1.17E-2			6.87	20	
Calcium	2.03E0	1.78E-3	"		2.06E0			1.40	20	
Potassium	9.11E-2	1.08E-2	"		9.26E-2			1.64	20	
Magnesium	9.61E-2	1.25E-4	"		1.08E-1			11.5	20	
Strontium	5.04E-3	5.19E-4	"		5.30E-3			4.89	20	
Sodium	6.36E-3	1.62E-3	"		5.88E-3			7.85	20	

Total Metals by PNNL-AGG-ICP-AES - Quality Control

Environmental Science Laboratory

Analyte	Result	Reporting Limit	Units	Spike Level	Source Result	%REC	%REC Limits	RPD	RPD Limit	Notes
Batch 1C16004 - CEC Extract (ICP/ICPMS)										
Duplicate (1C16004-DUP3)		**Source: 1103002-04**		Prepared & Analyzed: 03/16/11						
Barium	1.44E-2	1.34E-4	mg/g dry		1.42E-2			1.36	20	
Calcium	2.35E0	1.81E-3	"		2.34E0			0.496	20	
Potassium	1.04E-1	1.09E-2	"		9.64E-2			7.38	20	
Magnesium	3.51E-1	1.26E-4	"		3.43E-1			2.09	20	
Strontium	9.81E-3	5.25E-4	"		9.85E-3			0.402	20	
Sodium	1.78E-2	1.64E-3	"		1.63E-2			8.76	20	
Duplicate (1C16004-DUP4)		**Source: 1103002-03**		Prepared & Analyzed: 03/16/11						
Barium	1.16E-2	1.32E-4	mg/g dry		1.15E-2			0.743	20	
Calcium	2.03E0	1.79E-3	"		2.05E0			1.20	20	
Potassium	9.50E-2	1.08E-2	"		9.05E-2			4.85	20	
Magnesium	1.05E-1	1.25E-4	"		1.01E-1			4.04	20	
Strontium	5.12E-3	5.21E-4	"		5.19E-3			1.31	20	
Sodium	6.17E-3	1.63E-3	"		6.10E-3			1.23	20	
Post Spike (1C16004-PS1)		**Source: 1103002-04**		Prepared & Analyzed: 03/16/11						
Barium	5.62E2	N/A	ug/L	2.50E2	3.86E2	70.1	75-125			
Calcium	5.67E4	N/A	"	5.00E2	6.34E4	NR	75-125			
Potassium	3.75E3	N/A	"	1.25E3	2.61E3	91.4	75-125			
Magnesium	3.24E3	N/A	"	5.00E2	9.31E3	NR	75-125			
Strontium	6.58E2	N/A	"	5.00E2	2.67E2	78.2	75-125			
Sodium	6.88E2	N/A	"	5.00E2	4.42E2	49	75-125			

Physical Characteristics - Quality Control
Environmental Science Laboratory

Analyte	Result	Reporting Limit	Units	Spike Level	Source Result	%REC	%REC Limits	RPD	RPD Limit	Notes
Batch 2A24013 - CEC Extract Initial										
Duplicate (2A24013-DUP1)	**Source: 1103002-01**			Prepared & Analyzed: 01/24/12						
Cation-exchange capacity of soils	1.12E1	N/A	meq/100 g		1.15E1			2.22	200	
Duplicate (2A24013-DUP2)	**Source: 1103002-02**			Prepared & Analyzed: 01/24/12						
Cation-exchange capacity of soils	1.49E1	N/A	meq/100 g		1.42E1			4.68	200	
Duplicate (2A24013-DUP3)	**Source: 1103002-03**			Prepared & Analyzed: 01/24/12						
Cation-exchange capacity of soils	1.13E1	N/A	meq/100 g		1.13E1			0.487	200	
Duplicate (2A24013-DUP4)	**Source: 1103002-04**			Prepared & Analyzed: 01/24/12						
Cation-exchange capacity of soils	1.50E1	N/A	meq/100 g		1.49E1			0.950	200	

Particle Density - Quality Control
Environmental Science Laboratory

Analyte	Result	Reporting Limit	Units	Spike Level	Source Result	%REC	%REC Limits	RPD	RPD Limit	Notes
Batch 1C08016 - NO PREP (PHY CHAR)										
Blank (1C08016-BLK1)				Prepared: 03/09/11 Analyzed: 03/10/11						
Particle Density	0	N/A	g/cc							

Distribution

No. of Copies

ONSITE

3 **Washington Closure Hanford LLC**

SG Marske	L4-31
DJ McBride	L7-11
MW Perrott	H4-23

No. of Copies

7 **Pacific Northwest National Laboratory**

DH Bacon	K9-33
RE Clayton	K6-75
MJ Fayer	K9-33
VL Freedman	K9-36
MJ Lindberg	P7-54
RE Peterson	K6-75
ML Rockhold	K9-36

Pacific Northwest
NATIONAL LABORATORY

U.S. DEPARTMENT OF
ENERGY

Proudly Operated by Battelle *Since 1965*

902 Battelle Boulevard
P.O. Box 999
Richland, WA 99352
1-888-375-PNNL (7665)
www.pnl.gov